Lithos 210–211 (2014) 69–88

Contents lists available at ScienceDirect

Lithos

journal homepage: www.elsevier.com/locate/lithos

Extreme trace elements fractionation in Cenozoic nephelinites and phonolites from the Moroccan Anti-Atlas (Eastern Saghro)

Julien Berger [a,*], Nasser Ennih [b], Jean-Paul Liégeois [c]

[a] Géosciences Environnement Toulouse (GET), Observatoire Midi-Pyrénées, Université de Toulouse, CNRS, IRD, 14 avenue Edouard Belin, F-31400 Toulouse, France
[b] Laboratoire de Géodynamique, Université Chouaïb Doukkali, El Jadida, Morocco
[c] Geodynamics and Mineral Resources, Royal Museum for Central Africa, B-3080 Tervuren, Belgium

ARTICLE INFO

Article history:
Received 27 March 2014
Accepted 17 September 2014
Available online 30 September 2014

Keywords:
Peralkaline differentiation
Nb/Ta and Zr/Hf fractionation
Intraplate magmatism
Metasomatism
Circum-Mediterranean volcanism

ABSTRACT

Nephelinites and phonolites from the Moroccan Anti-Atlas form a cogenetic series of volcanic rocks linked by a fractional crystallization process and showing continuous evolutionary trends for trace-elements. According to partial melting calculations, minor element data in olivine and review of published experimental studies, the most primitive nephelinites are low degree (~2%) partial melts from a carbonated LREE-rich spinel lherzolite. Sr–Nd–Pb isotopic compositions indicate the participation of both DM and HIMU end-members in the mantle source of nephelinites; the HIMU component is here interpreted as a relic of the shallow metasomatized Pan-African mantle. The phonolites show similar isotopic composition except for slightly more radiogenic Sr isotopic values. Fractional crystallization calculations were performed using trace-element mineral/bulk rock coefficients determined with new LA-ICP-MS data on minerals together with published equilibrium partition coefficients. The decrease of LREE, Sr and Ba with increasing differentiation is explained by fractionation of large amounts of apatite. Th, Nb and Zr display a behavior of very incompatible elements, reaching extreme concentration in most differentiated phonolites. Ta, Hf and MREE by contrast are characterized by a moderately incompatible to compatible behavior during differentiation. Fractionation of small amount of titanite, in which Ta, Hf and MREE are highly compatible compared to Nb, Zr and LREE (DNb/DTa: 2, DZr/DHf: 1.5 for titanite/phonolite ratios), explains the observed increase in Nb/Ta and Zr/Hf ratios with increasing silica content, from 18 and 40 in nephelinites to 70 and 80 in phonolites, respectively. Clinopyroxene also contributed to the fractionation of Hf from Zr in the very first steps of crystallization. The low values of Nb/Ta and Zr/Hf ratios observed in the two most differentiated Si-rich phonolites are probably a consequence of late stage segregation of volatile-rich agpaitic assemblages in the underlying magma chamber. Two phonolites with extreme Sr contents plot outside fractionation trends, as a result of the remelting of previously crystallized nephelinitic rocks in depth.

1. Introduction

Ultrabasic, strongly alkaline primitive magmas are formed by low partial melting degrees in the mantle (Hirose and Kushiro, 1993), the latter being generally metasomatized (i.e., having experienced infiltration of melts or fluids with "exotic" chemical compositions; Downes et al., 2005; Pilet et al., 2008; Tatsumi et al., 1999). These alkaline melts are typically rich not only in incompatible trace elements but also in mobile components such as CO_2, H_2O, F and Cl. Peralkaline rocks are also characterized by a complex mineralogy (Sorensen, 1997) leading to unusual fractional crystallization trends. Fractionation of these mineral assemblages during differentiation of the peralkaline magma leads to the usual enrichment in some very incompatible elements in the melt but at the same time, depletion in trace elements that are usually considered as incompatible in other less alkaline to non-alkaline magmatic series can occur (Marks et al., 2008). As an example, fractionation of small amounts of apatite and titanite, that are characterized by high LREE and MREE mineral/melt partition coefficients (Olin and Wolff, 2012; Prowatke and Klemme, 2006), can lead to a continuous depletion of melt LREE and MREE contents during fractional crystallization (Marks et al., 2008). Very incompatible elements with similar geochemical characteristic (ionic charge and radius) have a generally similar mineral/melt partition coefficient and as a consequence, their ratios do not change significantly with the degree of partial melting and fractional crystallization (Hofmann and Jochum, 1996). This is particularly the case for the ratio of so-called geochemical twins, namely Nb/Ta and Zr/Hf (Pfander et al., 2007; Weyer et al., 2003). Recent studies however pointed out that in plutonic to subvolcanic alkaline–carbonatitic complexes, Nb/Ta and Zr/Hf ratios increase during differentiation (e.g., Marks et al., 2008), implying that the partition coefficients for both elements are not equal, especially when Ti-rich

* Corresponding author at: Université Paul Sabatier, Géosciences Environnement Toulouse (GET), 14, Avenue Edouard Belin, 31400 Toulouse, France. Tel.: +33 5 61 33 26 31.
E-mail address: julien.berger@get.obs-mip.fr (J. Berger).

http://dx.doi.org/10.1016/j.lithos.2014.09.018
0024-4937/

minerals are involved (Green and Pearson, 1987; Olin and Wolff, 2012). Other canonical ratios such as Ce/Pb and Nb/U are also used to estimate the proportion of recycled sedimentary components in the mantle source of primitive basalts (Hofmann, 1997). Differentiation can lead to modification of these ratios and their usefulness as proxies for the amount of recycled crust in the mantle source is biased; this is especially the case of the Si-undersaturated alkaline series such as in the Moroccan Anti-Atlas.

The Mio-Pliocene Saghro Cenozoic volcanic rocks in the Moroccan Anti-Atlas (Berrahma et al., 1993) are amongst the most Si-undersaturated and alkaline-rich volcanic rocks from the Circum Mediterranean volcanic province (Berger et al., 2009; Lustrino and Wilson, 2007). Nephelinites and phonolites are the dominant volcanic products, the former contains scarce wehrlite, pyroxenite and carbonatite xenoliths while the latter frequently shows syenite inclusions (Berger et al., 2009; Ibhi et al., 2002). The nature of these xenoliths indicates that the Saghro lies atop an ultrabasic-alkaline-carbonatitic plutonic complex (Berger et al., 2009; Downes et al., 2005). In this study, new trace element data on bulk rocks and some minerals together with the Sr–Nd–Pb isotopic data are provided and processed to explain the formation of magma with extreme incompatible element concentrations and the fractionation of trace element ratios that are usually unmodified during differentiation.

2. Geological context of the Saghro volcanism

The Anti-Atlas uplifted area is located at the boundary between the thick lithosphere of the West African craton toward the South and Peri-Gondwanan-related terranes to the North (Fig. 1). This domain was successively affected by the Eburnean (~2.0 Ga), the Pan-African (760–545 Ma) and the Variscan (420–300 Ma) orogenies (Ennih and Liégeois, 2001, 2008; Gasquet et al., 2008; Hoepffner et al., 2005; Thomas et al., 2004). The Pan-African event led to the Neoproterozoic magmatic growth by granitoid production and ophiolite/island arc accretion and reworking of the Paleoproterozoic basement by deformation and metamorphism. The Variscan orogeny is only expressed by thick-skin tectonics leading to folding of the Paleozoic sedimentary formations and fracturing of the Precambrian basement (Burkhard et al., 2006). The Triassic to Cretaceous period is characterized by the formation of intra-continental rifts at the location of High Atlas and Middle Atlas, accompanied by Lower Jurassic magmatism (Bensalah et al., 2013, and references therein). The Mesozoic rifts were inverted during the Cenozoic and syn-tectonic sediments were deposited in adjacent sub-Atlasic belts and foreland basins (Frizon de Lamotte et al., 2000; Tesón and Teixell, 2008). According to apatite fission track data and modeling, the High- and Anti-Atlas belts underwent strong uplift during the Neogene (Malusà et al., 2007; Missenard et al., 2008). This uplift event cannot be fully explained by tectonic processes as shortening did not exceed 25% in the High-Atlas belt (Teixell et al., 2003) and because compressional structures (folds, inverse faults) are relatively scarce, as it is in the uplifted Anti-Atlas (Malusà et al., 2007). Modeling of geophysical and topographic data has successfully demonstrated that the elevated areas (Anti-Atlas, central High Atlas and Middle Atlas) lie above a thin lithosphere, characterized by an asthenosphere uplift up to 60 km depth and by the occurrence of alkaline Cenozoic volcanism (Teixell et al., 2005; Missenard et al., 2006; Urchulutegui et al., 2006; Fig. 1). The origin of the thermal uplift is difficult to constrain and it has been the subject to lively debates. It has been related to the horizontal propagation of the Canary plume under the Atlasic corridor (Duggen et al., 2009) but this interpretation has been questioned by Berger et al. (2010) as it does not integrate the Cenozoic geological evolution of the Atlas region and the age distribution of Moroccan volcanism. Recently, Missenard and Cadoux (2012) have proposed that edge-driven convection at the northernmost boundary of the

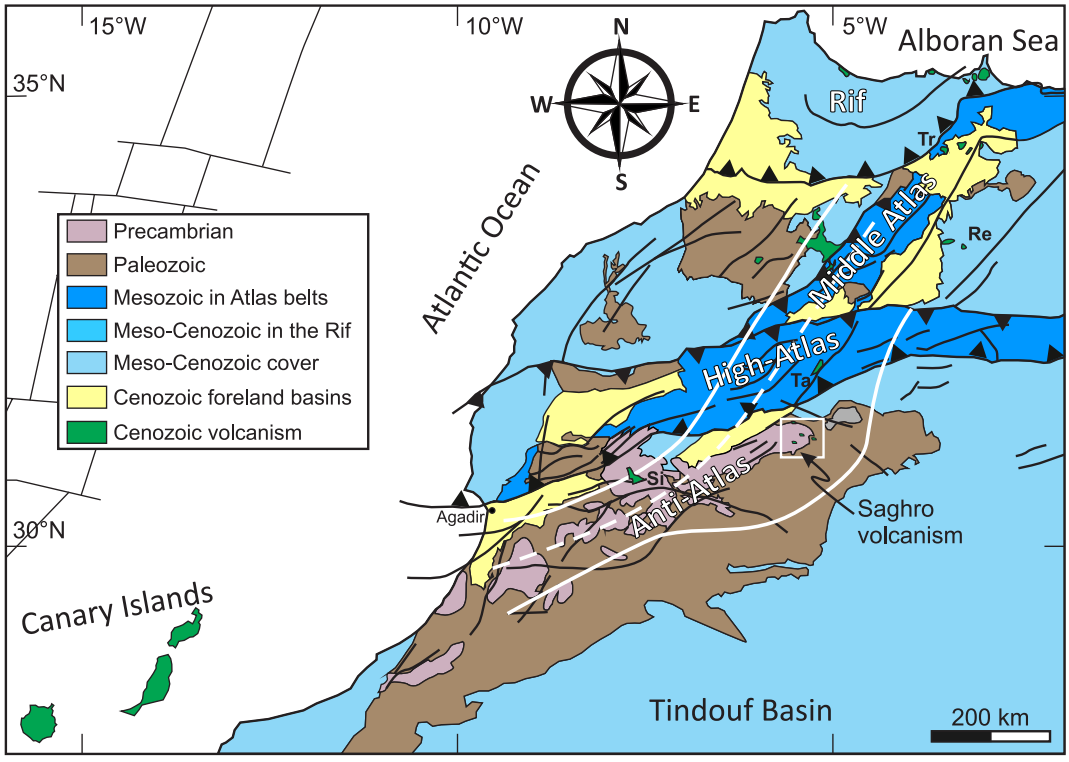

Fig. 1. Simplified geological map of Morocco and bordering regions showing the location of Cenozoic volcanic units. The discontinuous line is the 60 km isodepth contour of the top of the lithospheric anomaly while the continuous lines are representing the 100 km depth for lithosphere–asthenosphere boundary (from Missenard et al., 2006). Re: Rekkame, Si: Siroua, Ta: Tamazight, Tr Taourirt.

thick West-African cratonic lithosphere induces the lithospheric thinning below the Anti-, High and Middle Atlas areas; lithospheric delamination also probably played a role (Bezada et al., 2014).

Neogene alkaline volcanic rocks have been erupted between 11 and 2 Ma in the Anti-Alas (Berrahma and Delaloye, 1989; Berrahma et al., 1993) during the main tectonic and thermal uplift in the adjacent High-Atlas belt. These lava flows and domes are now forming topographic peaks meaning that erosion took place also after cessation of volcanic activity and that uplift is still an ongoing process (Malusà et al., 2007). Early Cenozoic alkaline-carbonatitic igneous activity is recorded within the High-Atlas belt (Tamazeght complex, 40–35 Ma, Harmand and Cantagrel, 1984) and to the north of High-Atlas, namely the Rekkame nephelinites and basanites (50–32 Ma; Rachdi et al., 1997) and the Taourirt carbonatite–alkaline complex (67–35 Ma; Wagner et al., 2003; Fig. 1). Neogene to Quaternary alkaline volcanic to subvolcanic rocks are also present in the Middle Atlas, the Central Morocco and in the Rif belt (see Lustrino and Wilson, 2007 for a review).

3. Main petrographic features of the Saghro lavas

The Saghro nephelinites and phonolites form lava flows and domes generally associated with pyroclastic deposits. Flows contain rare small xenoliths of lherzolite, wehrlite, pyroxenite and carbonatite in the nephelinites (Ibhi et al., 2002) and titanite-bearing nepheline-syenites in the phonolites (Berger et al., 2009). Nephelinites are either characterized by the dominance of olivine phenocrysts (olivine–nephelinite) or augite phenocrysts (pyroxene–nephelinite). Their matrix is holocrystalline and formed by a network of augite, nepheline, Ti-magnetite, apatite, and perovskite with melilite found only in one sample (melilite nephelinite TAF 7). Carbonate-rich domains containing apatite and Ba-rich biotite (up to 20% BaO) were observed in a pyroxene–nephelinite and as inclusions into olivine phenocrysts (Berger et al., 2009). Phonolites are holocrystalline and dominated by sanidine, nepheline and green augite-aegirine phenocrysts with a groundmass made of sanidine, nepheline, aegirine, titanite, sodalite–nosean–hauyne and minor amounts of lorenzenite, hainite, eudialyte-like minerals and delhayelite in some peralkaline phonolites (Berger et al., 2009). The most Si-rich phonolites (IK and ELB samples) are composed of sanidine, nepheline and aegirine only. One intermediate rock containing phenocrysts from both nephelinites (pyroxenes and olivine) and phonolites (feldspar and nepheline) form a flow in the central part of the volcanic area. The phenocrysts of this sample are strongly resorbed with the development of reaction coronas. Table 1 summarizes the geochemical composition of the samples used in this study; more detailed descriptions and major element compositions of the minerals can be found in Ibhi et al. (2002) and Berger et al. (2008, 2009).

The alkaline lava suite from Saghro lacks rocks with intermediate composition (one sample with SiO_2 above 45 wt.% and below 52 wt.%; Berger et al., 2009; Berrahma et al., 1993). The numerous clinopyroxene xenocrysts in nephelinites have crystallized in magmas having intermediate composition between nephelinites and phonolites (Berger et al., 2008, 2009) attesting that these intermediate magmas exist at depth but were not erupted. This and the close similarities between the mineralogy and bulk chemical composition of modeled cumulates and those forming ultramafic-alkaline-carbonatitic complexes (Downes et al., 2005) have been interpreted as evidences for a polybaric fractional crystallization linkage between nephelinites and phonolites (Berger et al., 2008, 2009).

For simplicity, the two phonolite samples with anomalously high Sr contents will be named Sr-rich phonolites (TO and OUL) while the two phonolites with the highest silica content will be labeled Si-rich phonolites (IK and ELB). All other phonolites will be referred to as peralkaline.

4. Major and trace elements geochemistry

Major element analyses (Table 1) were presented in Berger et al. (2009) to discuss about the mineral/melt equilibrium in nephelinites and phonolites. They are used in this paper to support the trace element based fractional crystallization study and to compare the Saghro volcanics to other North African Mio-Pliocene alkaline lavas. The nephelinites (37–43 wt.% SiO_2, all silica and other oxides cited hereafter have been recalculated on a anhydrous basis) range from primitive (14 wt.% MgO) to evolved (8 wt.% MgO) magmas with high Ca (11–15 wt.% CaO) and low Al contents (11–13.5 wt.% Al_2O_3). The most primitive nephelinites are comparable, in terms of major elements, to Cenozoic Si-undersaturated alkaline magmas from the Rekkame area (Rachdi et al., 1997), in the Middle Atlas (Duggen et al., 2009) but also on Gran Canaria in the Canary Islands (Hoernle and Schmincke, 1993; Fig. 2). By contrast, nephelinites are not present in the adjacent and contemporaneous Siroua strato-volcano in the central Anti-Atlas (Berrahma and Delaloye, 1989), which is characterized by the presence of primitive basanites (Fig. 2).

The Si content of phonolites varies from 52 to 58.5 wt.% SiO_2 (Fig. 2) while the Na_2O values range from 8.6 to 10.8 wt.%, with significantly lower values for two altered phonolites (6 and 8 wt.% LOI). Al contents are high (19–21 wt.% Al_2O_3) compared to nephelinites and MgO gently decreases with increasing Si content from 2.5 wt.% (TAB 1) to 0.2 wt.% (IK 01). The same trend is also observed for CaO. The Saghro lavas are amongst the most alkali-rich and silica-undersaturated series when compared to Canary Islands and Middle Atlas (Fig. 2).

Most trace elements display regular correlations with silica and often an incompatible behavior with sometimes extreme range of variations (Fig. 3, Table 1). For example, Zr increases from 210 ppm in the nephelinites to 2100 ppm in the phonolites, Th increase from 14 to 87 ppm and Nb ranges from 120 to 570 ppm.

Ba, Sr, LREE, MREE, Ta and light transition elements (e.g., Cr, Co, Ni) show decreasing to stagnant values with increasing silica (Fig. 3, Table 1). Sr ranges from 2100 ppm in the nephelinite TAF 7 to 87 ppm in the phonolite IK 01 (with the exception of two samples having much higher Sr than other phonolites, 2500–3000 ppm, Table 1); Ta decreases from primitive to evolved nephelinites (10–6 ppm) while the concentration is scattered for phonolites (3–12 ppm, Table 1), the two Si-richest phonolites showing the highest enrichment in Ta. Nb/Ta ratios are consequently increasing from 18 in the nephelinites up to 69 in the nephelinites (Fig. 4). Hf is slightly less incompatible than Zr during differentiation of the nephelinite magma into phonolites which results in an increase in the Zr/Hf ratio with increasing silica, from 38 to 82 (Fig. 4). These two ratios are however lower for the two most differentiated, Si-rich phonolites than for the most evolved peralkaline phonolites. Trace element ratios commonly used to estimate the fraction of recycled sediments into the mantle source are strongly dependent of the degree of fractionation, Nb/U and Ce/Pb range from 50 in the nephelinites to 18 and 2, respectively in the phonolites (Fig. 4).

Heavy rare earth elements (e.g., Yb) and Y behave like compatible elements for low silica contents (Fig. 3), before getting a incompatible behavior, reaching minimum values at 45–50 wt.% SiO_2. The most Si-rich phonolites show the highest contents in HREE and Y.

Nephelinites are characterized by a steep LREE-enriched linear pattern in CI chondrite-normalized plots (Fig. 5a). They show maximum primitive mantle-normalized abundances for the most incompatible elements (Rb, Ba, Th, U, Nb, Ta) with comparatively low values for HREE, Zr, Hf and Y (Fig. 5b). They also show negative spikes for Rb, K and Pb, a common feature of magma derived from a HIMU mantle (e.g., Panter et al., 2006). The trace element fingerprint is very close to Middle Atlas basanites and nephelinites, Canary Islands nephelinites and Early Cenozoic Rekkame nephelinites (Fig. 5b) although the Saghro

Table 1
Major and trace-element composition of bulk volcanic rocks from Saghro. XY coordinates in UTM.

Rock	Nephelinites					Phono	Phonolites		Phonolites								Phonolites		SRM	SRM
Type	Mel-Ol	Ol	Ol	Px	Px	Tephrite	Sr-rich		Peralkaline								Si-rich		Measured	Reference
UTM X	284123	247239	282543	247835	252725	260376	253190	253821	252725	268337	257063	255547	257828	255453	264856	252725	245072	274015		
UTM Y	3471452	3481114	3444311	3480617	3441892	3452572	3444177	3448039	3441892	3445472	3442002	3443905	3442104	3440209	3438132	3441892	3450847	3435186		
Sample	TAF 7	FN 4	TL 6	FS 5	TAB 3	AS 1	OUL 3	TO 1	TAB 1	TG 1	AZLOU 1	TIM 1	SAR 3	BAG 2	MIG 2	TAB 7	IK 01	ELB 6	BR	BR
wt.%																				
SiO_2	37.24	39.30	39.02	39.68	42.75	47.75	50.27	52.42	49.99	52.20	52.58	52.80	54.40	54.30	54.92	54.38	54.65	55.51		
Al_2O_3	11.83	10.67	10.84	11.37	13.61	16.42	21.30	21.53	19.21	19.77	19.56	20.68	19.90	20.95	20.69	20.37	20.16	20.81		
Fe_2O3t	12.75	11.72	12.35	11.71	10.64	7.46	3.85	4.47	4.80	5.22	4.99	4.08	4.27	3.62	3.76	3.59	3.78	2.89		
MnO	0.23	0.19	0.18	0.21	0.18	0.19	0.14	0.15	0.17	0.20	0.22	0.18	0.24	0.19	0.22	0.20	0.22	0.21		
MgO	10.04	13.96	13.18	10.30	8.40	4.76	0.65	0.58	2.44	1.25	1.23	0.78	0.39	0.29	0.31	0.15	0.20	0.34		
CaO	14.51	13.32	14.35	15.37	10.98	7.92	3.74	2.53	4.63	3.09	2.91	2.67	1.77	1.78	1.36	1.10	0.88	0.89		
Na_2O	3.81	3.41	2.80	3.06	4.45	6.19	5.70	7.86	8.33	9.42	10.38	8.93	9.08	9.63	10.60	9.22	8.86	9.83		
K_2O	2.06	1.94	1.31	1.73	3.15	4.03	7.71	7.69	6.06	6.10	5.13	6.52	6.71	6.61	5.65	6.95	4.54	5.09		
TiO_2	3.48	2.76	2.93	2.76	2.80	1.81	0.68	0.89	0.98	0.90	0.91	0.71	0.47	0.48	0.49	0.32	0.36	0.25		
P_2O_5	2.05	1.16	1.76	1.64	0.88	0.58	0.06	0.12	0.17	0.21	0.22	0.09	0.02	0.06	0.03	0.31	0.00	0.00		
LOI	1.19	1.84	1.42	2.67	1.19	2.06	6.88	2.25	2.15	1.21	0.70	1.21	2.15	1.52	0.80	3.34	5.12	3.65		
TOTAL	99.20	100.26	100.16	100.50	99.03	99.18	100.99	100.50	98.93	99.58	98.83	98.65	99.39	99.44	98.82	99.94	98.77	99.44		
ppm																				
V	295	230	281	231	245	151	78	83	122	84	81	70	71	65	41	46	20	15	253	235
Rb	48	50	43	52	75	117	176	161	209	191	214	226	246	216	276	229	251	324	46	47
Sr	2099	1283	1753	1915	1532	1390	2993	2591	1100	1286	838	1295	868	948	464	540	87	142	1322	1320
Y	39	27	31	34	24	29	15	19	22	24	39	17	26	21	23	19	23	23	29	30
Zr	415	216	269	296	415	756	478	390	871	944	1541	951	1175	999	1377	936	1750	2101	260	250
Nb	187	128	159	169	148	275	192	213	307	339	404	266	352	303	369	247	572	533	99	98
Ba	1274	1151	1122	1746	1093	1148	1966	1772	811	752	732	816	347	416	213	49	36	56	1049	1050
La	164	98	130	131	88	126	94	106	83	97	186	75	77	75	77	101	35	119	79	85
Ce	283	169	226	230	148	193	121	146	129	141	253	103	113	110	103	119	56	142	149	151
Pr	30	20	26	27	16	20	9.7	13.7	12.2	13.6	20.5	8.7	9.4	9.5	8.1	8.3	4.8	10.0	17.3	17
Nd	113	69	88	91	59	58	29	37	42	38	61	27	28	28	23	22	12	26	66	65
Sm	17.9	13.4	14.4	15.5	9.9	9.2	4.2	5.6	6.3	5.8	8.0	4.0	4.0	3.8	3.2	2.6	2.0	3.0	13.1	12
Eu	5.28	3.85	4.29	4.90	3.03	2.67	1.32	1.72	1.89	1.78	2.26	1.14	1.20	1.17	0.89	0.70	0.70	0.74	3.6	3.7
Gd	13.66	10.14	10.95	12.87	8.03	7.20	3.66	4.64	5.64	5.02	6.89	3.25	3.82	3.66	2.90	2.18	2.37	2.41	9.8	9.5
Dy	9.05	5.91	6.33	7.01	5.52	4.77	2.63	3.01	4.24	3.92	5.88	2.99	3.97	3.39	3.28	2.65	2.69	3.12	6.2	6.2
Ho	1.49	0.99	1.11	1.17	0.92	0.91	0.53	0.59	0.81	0.79	1.24	0.61	0.85	0.72	0.74	0.61	0.64	0.73	0.99	1.1
Er	3.63	2.33	2.50	2.79	2.23	2.44	1.57	1.72	2.21	2.28	3.75	1.86	2.69	2.22	2.42	1.96	2.31	2.45	2.5	2.4
Yb	2.85	2.09	2.22	2.50	1.86	2.72	1.68	2.00	2.43	3.00	4.63	2.40	3.35	2.87	3.46	2.64	4.17	3.92	1.76	1.9
Lu	0.37	0.28	0.29	0.33	0.22	0.43	0.22	0.30	0.32	0.45	0.69	0.34	0.48	0.41	0.52	0.38	0.71	0.60	0.24	0.3
Hf	7.4	5.1	5.9	6.0	7.0	13.0	5.8	6.2	11.3	14.4	21.7	13.4	15.0	13.8	17.2	11.9	28.3	29.8	5.1	5.4
Ta	10.3	6.8	8.6	9.0	7.2	9.4	5.2	7.0	8.2	8.0	11.5	6.0	6.0	6.7	7.1	3.5	10.7	11.3	5.9	6.2
Pb	5.6	4.4	5.1	7.1	5.4	17.0	9.8	31.2	13.1	19.2	31.1	20.7	22.6	19.2	24.5	20.0	31.6	35.0	7	8.0
Th	17.1	13.8	14.9	16.7	13.7	36.2	20.7	21.0	35.3	41.2	71.0	35.3	50.8	41.6	57.5	39.1	83.2	87.4	11.6	11
U	3.8	3.0	3.4	3.7	3.2	10.0	6.5	8.4	10.2	13.3	12.5	10.1	15.0	12.7	18.9	11.7	23.7	28.9	2.7	2.5

nephelinites have the highest contents in very incompatible elements (Th, U, Nb, Ta, LREE).

Phonolites can be splitted into two groups regarding their REE pattern (Fig. 5c, e): a first group shows a flat HREE profile with normalized concentration increasing from MREE to LREE; the second group, comprise the two Si-richest phonolites, with a concave upward pattern characterized by slightly higher normalized values for Yb and Lu compared to other HREE (Fig. 5e). The differences between the two phonolite types are also observed in multi-elemental plots (Fig. 5 d, f): those with concave upward REE pattern are strongly depleted in Ba and P compared to the phonolites with the flat HREE profile. The latter also have lower concentrations in Th, U, Nb and Zr.

5. Sr–Nd–Pb isotopic geochemistry

Nephelinites form a restricted range of initial isotopic composition: $^{143}Nd/^{144}Nd$ from 0.51282–0.51287 (corresponding to ε_{Nd} values of +4.4 to +4.9), $^{87}Sr/^{86}Sr$ from 0.7030–0.7033, and 19.41–19.56, 15.61–15.63, 39.11–39.30 for $^{206}Pb/^{204}Pb$, $^{207}Pb/^{204}Pb$ and $^{208}Pb/^{204}Pb$ respectively; Fig. 6, Table 2. The less radiogenic Sr composition combined with radiogenic Pb and Nd signatures implies the involvement of the depleted mantle (DM, represented on Fig. 6 by Atlantic MORBs from same latitudes, data from the online PetDB database) and HIMU components in the source of nephelinites with negligible influence of enriched mantle (EM) end-members (Hofmann, 1997). This composition, close to FOZO, is typical of the North African Cenozoic alkaline volcanic province and oceanic islands (Fig. 6), including the Moroccan Middle Atlas (Duggen et al., 2009; Bosch et al., 2014), the Algerian Hoggar (Ait-Hamou et al., 2000; Allègre et al., 1981; Maza et al., 1998), volcanism in Northeastern Africa (Sudan and Egypt; Lucassen et al., 2008), the Canary Islands (Lustrino and Wilson, 2007) and the Cape Verde islands (GEOROC database). Phonolites have similar Nd and Pb isotopic compositions than nephelinites but slightly higher for Sr (0.7033–0.7037). The two Si-rich phonolites IK and ELB are characterized by more radiogenic $^{87}Sr/^{86}Sr$ (0.7056–0.7071) and one peralkaline phonolite with anomalous Sr concentration (2500 ppm) has low $^{206}Pb/^{204}Pb$ value (18.96) compared to remaining samples but also slightly lower values for the two other isotopic ratios (Fig. 6, Table 2).

6. LA-ICP-MS analyses on minerals and determination of mineral/bulk-rock coefficients

Trace element analyses on minerals have been performed on one sample of pyroxene nephelinite (FS) and four phonolites (TO, TIM, BAG, IK; Table 3). They were used to estimate mineral/bulk rock coefficients and are presented in Table 4 and Fig. 7. In the nephelinite, only clinopyroxene has been analyzed for technical reasons: this is the only mineral having its trace element content above detection limits and with many grains larger than the ablation spot size (~100 μm). Nepheline, apatite, melilite, perovskite and titanomagnetite in the groundmass are too small to be analyzed with a laser probe. For the same reasons, only clinopyroxene, titanite, nepheline and K-feldspar were analyzed in the phonolites.

Clinopyroxene has a typical trace element pattern characterized by low normalized contents in Nb, Ta and Sr and decreasing abundances from highly to slightly compatible elements (Fig. 7). The augite from the FS nephelinite has the lowest incompatible element contents, except for MREE. Aegirine–augite in the phonolites have higher incompatible element contents, except MREE in sample TO. However, two pyroxenes from the phonolites have similar trace element patterns than those from the nephelinite, suggesting that these two grains are xenocrysts in the phonolite. They were not used for the calculation of mean mineral/bulk rock ratios. Titanite is extremely rich in trace elements, especially Nb (up to 7000 ppm), Ta (up to 350 ppm) and LREE (up to 3200 ppm Ce). It shows decreasing normalized abundances from the left to right with negative spikes for Sr, Zr and Hf (Fig. 7).

Clinopyroxene and feldspar show strong major-element composition variation within single grains or between different grains of the same sample. For the estimation of mineral/bulk rock coefficients, we have only analyzed grains or zonations that are in effective chemical equilibrium with host lava major-element composition (see Berger et al., 2009). Despite this selection procedure, the determined values for mineral/bulk rock coefficients can vary significantly for a single lava sample, especially for clinopyroxene (Fig. 7). This is due to variation in trace element composition of minerals even at micro-scale (see standard deviation values in Table 3). It can be interpreted as evidence for local trace element disequilibrium between mineral and host lava and to the presence of xenocrysts, despite our careful selection based on major-elements.

Clinopyroxene in nephelinite FS shows a flat REE mineral/bulk rock ratio profile between La and Sm but decreasing ratio from Sm to Yb (Fig. 7). The mineral/bulk rock ratios for REE are <1, increasing from La (0.07–0.08) to Gd (0.48–0.57; see means in Table 4) then gently decreasing to Yb (0.29–0.37). All other trace elements are also incompatible in clinopyroxene lattice except Hf which has values around 1. Sr and Zr are moderately incompatible (0.12–0.16 and 0.47–0.67, respectively) while Nb and Ta are strongly incompatible with Ta having partition coefficient values (0.03–0.06) more than twice those of Nb (0.01–0.02, see means in Table 4). Using the microprobe data published in Berger et al. (2009) on the same samples, the determined coefficients between apatite and nephelinite range from 9 to 16 for Sr, 7 to 10 for Ce and 3 to 5 for Ba. For perovskite we have obtained coefficients between 90 and 110 for Ce, between 4 and 5 for Sr and ranging from 60 to 90 for Nb.

The clinopyroxene/bulk rock ratios determined for phonolites are strongly variable from one sample to another. Clinopyroxene from phonolite BAG is strongly zoned with respect to trace elements; this phase was thus considered to be out equilibrium with host bulk composition. Clinopyroxene from sample TO shows increasing partition coefficients from La to Yb (from 0.6 to 1) and very low coefficient for Nb and Ta. Similar to what was observed for nephelinites, the coefficient for Hf and Ta is twice those for their geochemical twins (Zr and Nb). Sample TIM

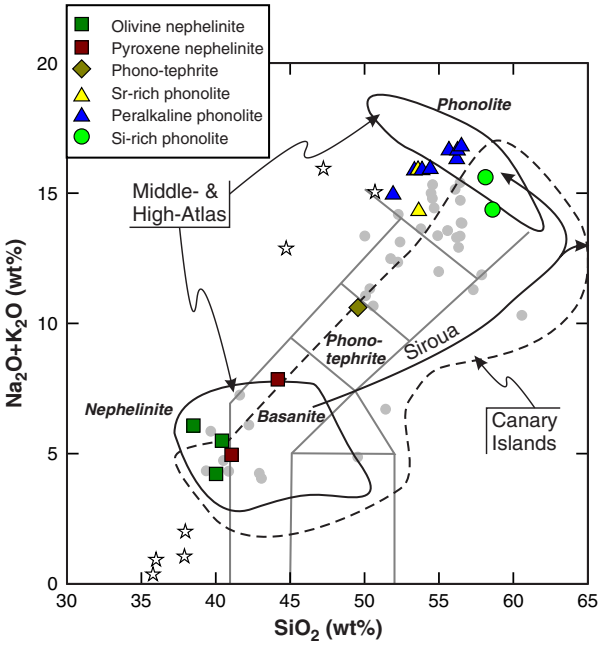

Fig. 2. TAS diagram (data recalculated on an anhydrous basis) from the Saghro volcanic rocks. Comparison data are from the online GEOROC database. The stars represent the composition of cogenetic cumulates calculated using major element data (Berger et al., 2009).
The gray dots are the major element composition of Saghro lavas presented by Berrahma et al. (1993).

shows a convex upward pattern for REE partition coefficients, with values up to 3.1 for Gd. This sample shows many evidence for re-equilibration of clinopyroxene phenocrysts with a late-stage, volatile-rich peralkaline melt (Berger et al., 2009); the determined coefficient was thus not used for further modeling.

Titanite/phonolite ratios are above unity for most measured elements (see Table 4), except Rb (close to detection limits). The REE coefficient profile is concave upward (Fig. 7) with maximum values for Sm (up to 40). Ta is strongly compatible in titanite lattice (ratio from 30 to 50), twice more than Nb (17–23). Hf coefficients (3–7) are usually higher than those determined for Zr (2–5).

7. Discussion

7.1. LREE-enriched carbonated lherzolite as a source for primitive nephelinite

Mantle-derived alkaline lavas can originate either from melting of pyroxenites or peridotite. The following discussion will sequentially: (i) use results of minor element analyses in primitive olivine from nephelinites; (ii) provide partial melting calculations to estimate the nature of the source of most primitive nephelinites; and (iii) review published experimental studies on the origin of nephelinites. All the

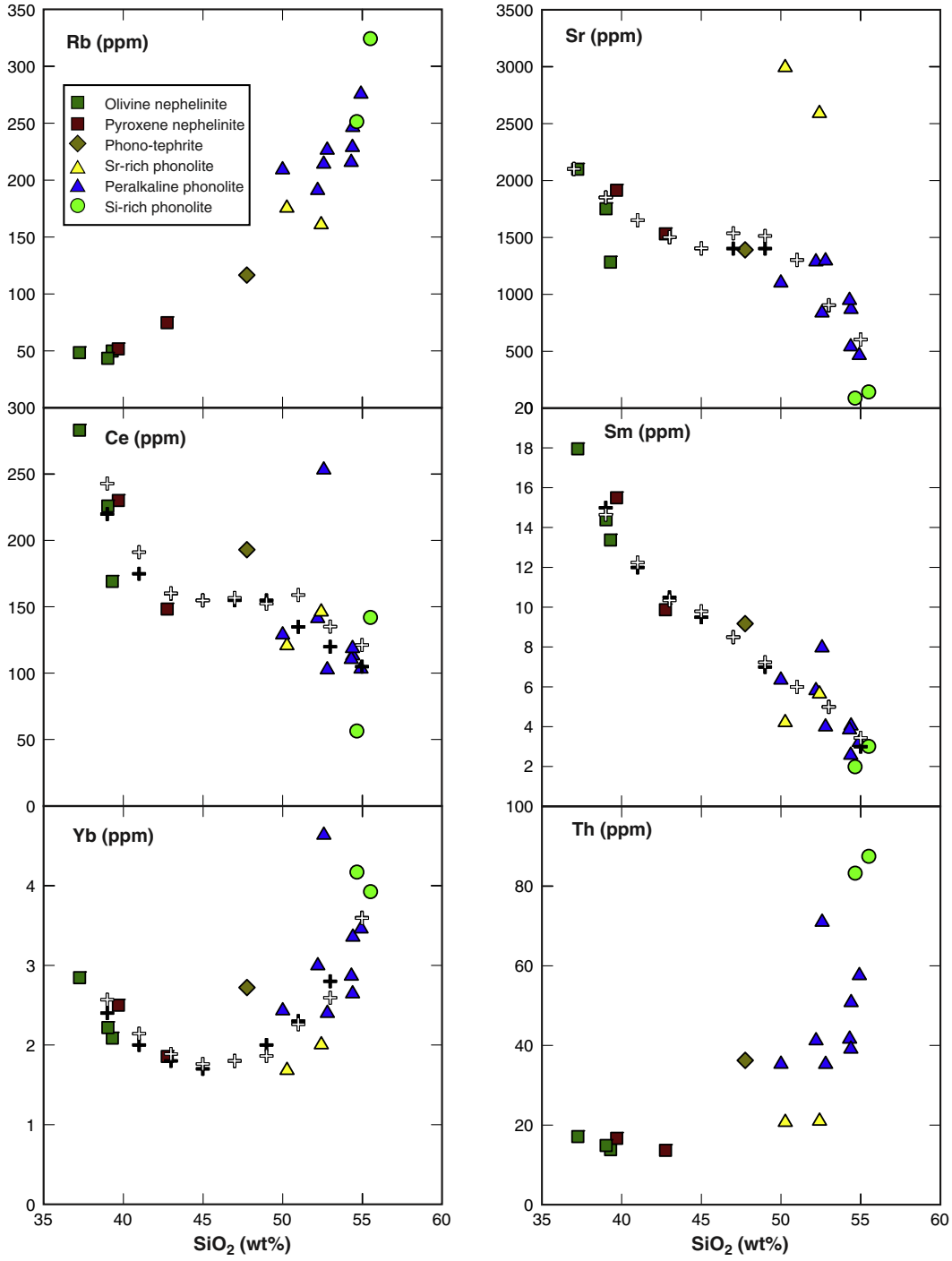

Fig. 3. Trace element (in ppm) vs SiO_2 plots for the Saghro volcanic rocks. White crosses are steps chosen for simulation of fractional crystallization, black crosses are the calculated ones.

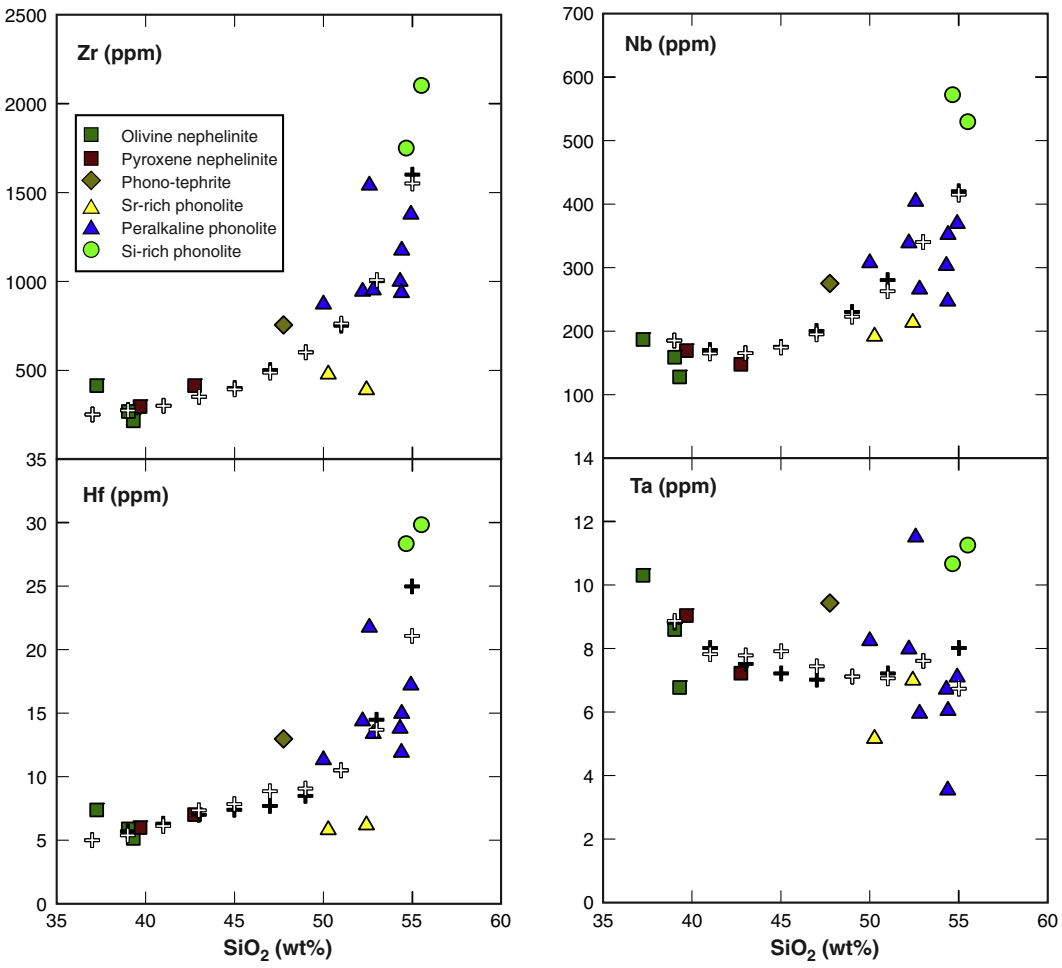

Fig. 3 (*continued*).

results acquired with the different approaches will be merged to infer the petrological nature of the mantle source and the partial melting process.

Sobolev et al. (2007) proposed a parameterization to compute the amount of recycled pyroxenites in the source of mantle-derived basaltic magmas using minor element distribution in olivine. Herzberg (2011) noted that the composition of mantle pyroxenites and peridotites varies considerably and that the parameterization of Sobolev et al. (2007) is oversimplified and does not take into account possible compositional variations of end-members. However, the Fe, Ni, Ca and Mg contents of primitive olivine phenocrysts can be used to qualitatively constrain if the mantle source is dominated by pyroxenite or peridotite. First, only the most primitive olivines should be selected because early fractionation lowers Ni contents in the magma and increases Ca, Mn and Fe/Mn ratio. Olivines with forsterite contents below 85 mol% show a marked decrease in Ni contents and an increase in Ca, Mn and Mn/Fe (Fig. 8); i.e. proxies that are used to infer the presence of pyroxenite in the source. These variations are consistent with early olivine fractionation in the magma (Herzberg, 2011). Accordingly, only the olivines with Fo content above 85 mol% can be used to infer the nature of the mantle source. Olivines from Saghro have low Ni contents (1000–2300 ppm), high Ca (1700–2400 ppm) and high but variable Mn/Fe ratios (Fig. 8). The latter cannot help to estimate the nature of the mantle source as it varies from pyroxenite to peridotite source values (Fig. 8). Melting of pyroxenite, in which Ni is less compatible than in olivine-rich sources, produces melt that is rich in Ni (Herzberg, 2011; Sobolev et al., 2007). Peridotite-derived melt thus crystallizes primitive olivine with Ni contents below 2500–3000 ppm while pyroxenite-derived melt crystallizes primitive olivine with Ni above 2500 ppm (Herzberg, 2011; Sobolev et al., 2007). The Ni contents in Saghro olivine with Fo > 85 mol% is 780–2300 ppm Ni (0.10–0.30 wt.% NiO) corresponding to a fractionation-normalized Ni/(Mg/Fe)/1000 ratio of 0.3–0.6 that is typical of olivine-dominated peridotite sources (Fig. 8).

To further constrain the nature of the peridotitic source, the trace element signature of the most primitive nephelinite TAF 7 has been simulated using classical equations for non-modal batch and aggregated fractional melting (Shaw, 1970). They are:

$$C_{liq} = \frac{C_{sol}}{\mathrm{F} * (1-\mathrm{P}) + \mathrm{D}} \text{ for batch melting}$$

$$C_{liq} = \frac{C_{sol}}{\mathrm{F}} \left[1 - \left(1 - \frac{\mathrm{P} * \mathrm{F}}{\mathrm{D}}\right)^{1/\mathrm{P}}\right] \text{ for aggregated fractional melting}$$

where C_{liq} is the concentration in the partial melt, C_{sol} is the concentration in the starting solid material, F is the degree of melting (weight fraction of melt), P is the bulk partition coefficient for phases participating to melting and D is the bulk partition coefficient for the initial source.

To perform this calculation, the composition of plausible source peridotite and mineral/melt partition coefficients is required from published studies while other parameters are adjusted by successive iteration. These are the initial weight fraction of minerals in the source

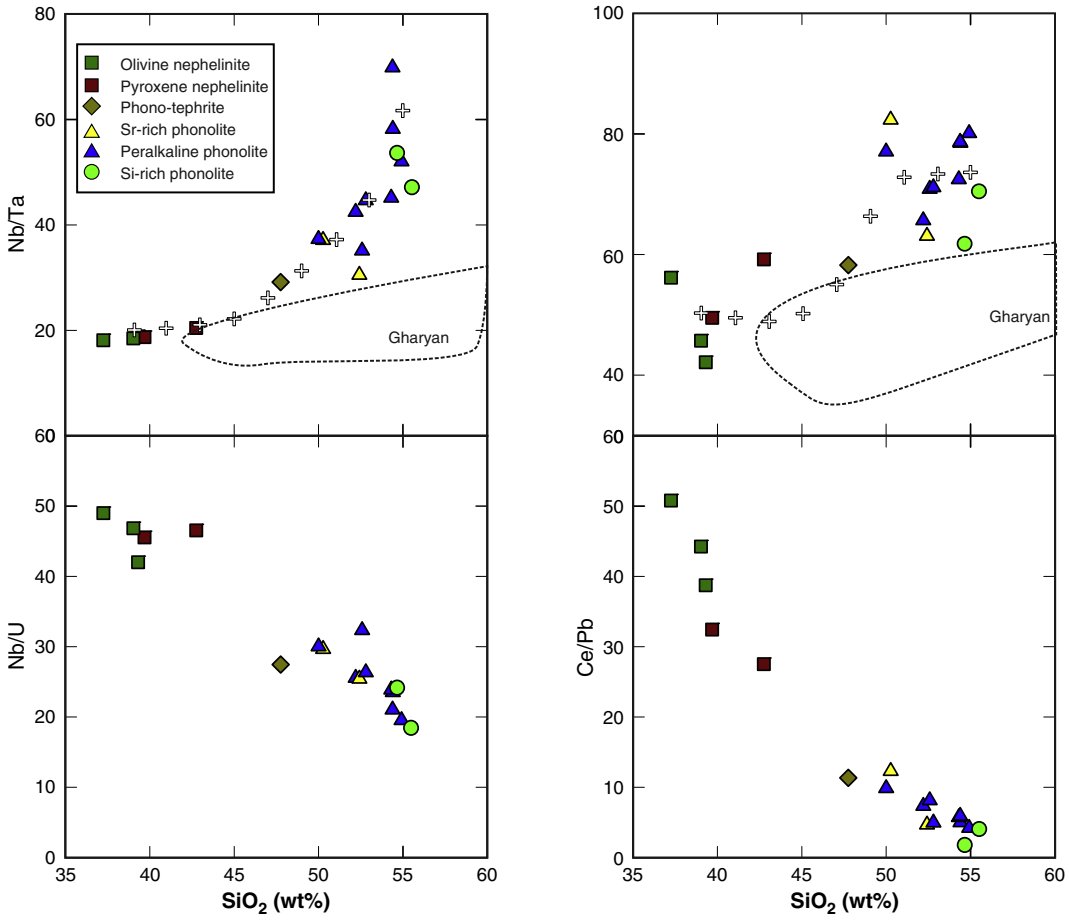

Fig. 4. Evolution of trace-element ratios with increasing silica contents. White crosses are the results from fractional crystallization simulations.

(used to compute the initial bulk partition coefficient D), the weight proportion of phases effectively participating to melting (used to compute the coefficient P) and the weight fraction of melt (F, also known as the degree of melting). Calculated REE concentrations in the partial melt were fitted to the measured ones by successive iterations while minimizing the residual sum of squares (RSS) between calculated and measured values. To avoid the over contribution of abundant REEs (such as La or Ce) in the value of the RSS, the square of the difference between calculated and measured values for each element was normalized to the measured concentration to give rise to the normalized RSS:

$$\mathrm{nRSS} = \sum_{i=1}^{n} \frac{(C_{meas} - C_{Calc})^2}{C_{meas}}$$

The fitting was done only for REE but the concentration of other elements (Rb, Th, U, Nb, Ta, Sr, Zr, Hf, Y) was also computed in order to have an independent complementary control on the validity of calculation results. Partition coefficient for olivine, orthopyroxene, clinopyroxene and spinel are those experimentally determined by McDade et al. (2003) for basalt/lherzolite equilibrium at 1.5 GPa (the missing coefficients for some REE have been extrapolated from surrounding elements). Coefficients for garnet (Hauri et al., 1994), phlogopite and amphibole (LaTourrette et al., 1995) were also used to test if these minerals were present in the source. The trace element composition of the mantle source below Saghro is unknown. Mantle xenoliths are very small and rare in the Saghro region and no information on their bulk composition is available, despite our expectations. A recent study (Natali et al., 2013) investigated mantle xenoliths from the Moroccan Middle Atlas where the Cenozoic volcanic rocks have the same geochemical characteristic and the same Cenozoic geological history that in Saghro (see Figs. 1 and 2, and Duggen et al., 2009). Three types of lherzolite characterize the Middle Atlas mantle: LREE-enriched lherzolite, REE-poor lherzolite and cpx-poor lherzolite with spoon-shaped REE pattern (Fig. 9 and Supplementary online Fig. A). The three types of lherzolites were tested in our calculations, they are represented respectively by samples AT 5, AT 10 and AT 12 from Natali et al. (2013).

The results of partial melting calculation are presented in Fig. 9, Supplementary online Fig. A and Table 5. The most statistically correct (nRSS for REE of 4.4) and significant results were obtained with the LREE-enriched lherzolite and the equation for batch melting (Table 5, Fig. 9). The source material was a lherzolite containing 61 wt.% of olivine, 29 wt.% of orthopyroxene, 9 wt.% of clinopyroxene and 1 wt.% spinel. The latter and orthopyroxene were the main contributors to non-modal melting (57 and 35 wt.%, respectively). Adding garnet, phlogopite or amphibole in the source systematically leads to an increase of nRSS for REE, meaning that these phases were probably not present in the source material or only in very minor proportions and that spinel was the stable Al-bearing phase in the source of Saghro nephelinites. The fractional melting calculations gave statistically less valuable (nRSS of 6.7) results but still meaningful (Fig. 9): the source is a garnet-free, spinel-bearing lherzolite and clinopyroxene is also the main contributor to melting (see Table 5 and Fig. 9). Both calculations gave very low degree of melting of 1.7 and 1.9 wt.% respectively, in agreement with experimental data for the production of nephelinites (Dasgupta et al., 2007) and high Ti contents (see below). Tests

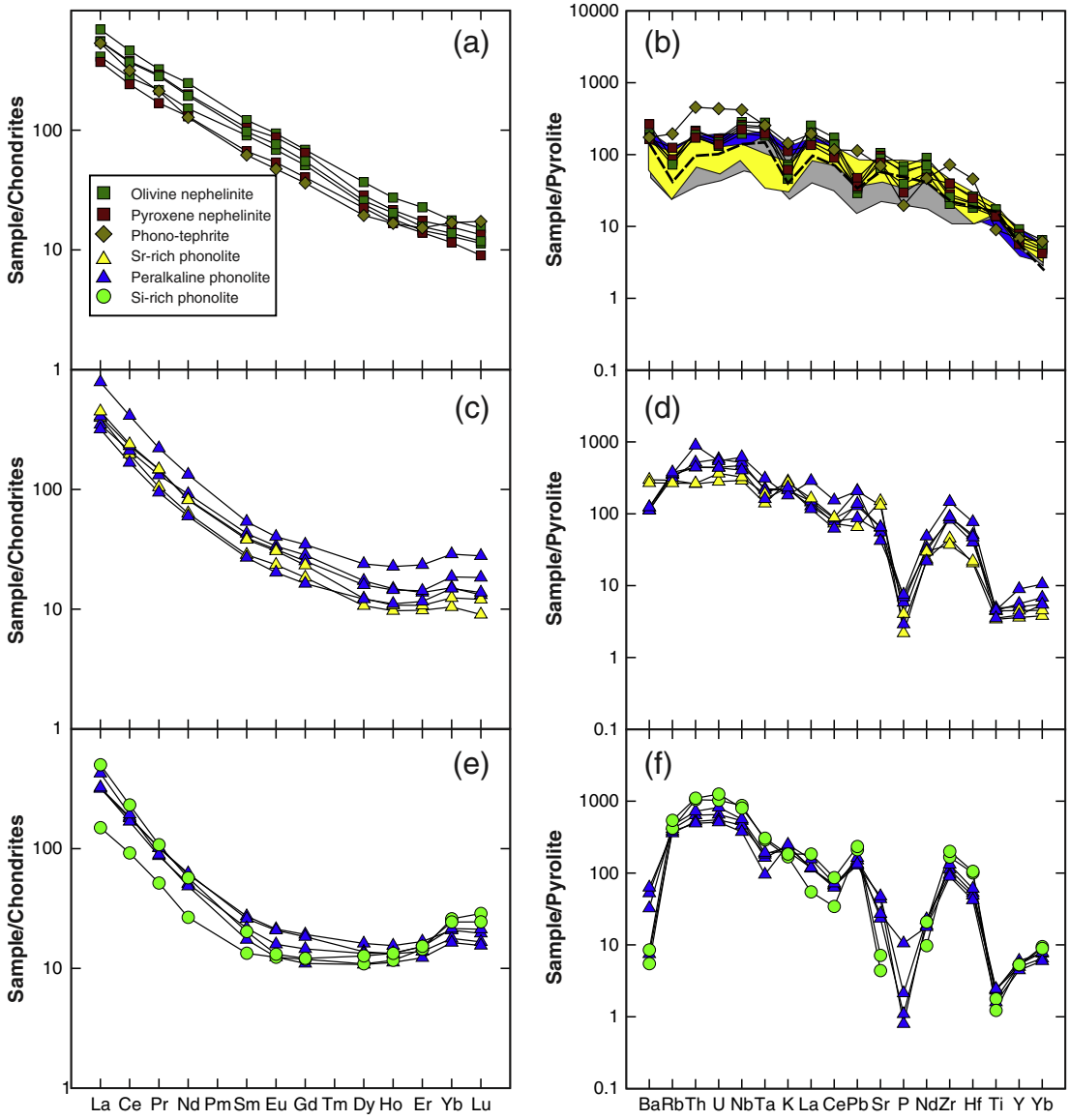

Fig. 5. REE patterns (a, c, e) and multi-element diagrams (b, d, f) from nephelinites and phonolites in Saghro. Field of primitive nephelinites and basanites from the Middle Atlas lava (blue field, Duggen et al., 2009), the Rekkame nephelinites (Rachdi et al., 1997) and the Taourirt nephelinites (Wagner et al., 2003) (both in the gray field), one Tamazight nephelinite (discontinuous line, Bouabdellah et al., 2010) and Gran Canaria nephelinites/basanites (yellow field, data from the online GEOROC database) are shown for comparison. (For interpretation of the references to color in this figure legend, the reader is referred to the web version of this article.)
Normalization values from McDonough and Sun (1995).

performed with the cpx-poor and the REE-poor lherzolites (see Supplementary online material) did not lead to a good convergence (nRSS for REE of 15.9 and 47.3, respectively) and produced meaningless results: extremely low F (<0.006), melting of clinopyroxene from a clinopyroxene-free source or melting of olivine only (see Supplementary online Fig. 1). The concentration of other trace elements was globally well reproduced by the batch melting of the LREE-enriched lherzolite (see Fig. 9 and Table 5), except for Sr. The sample AT 5 from Natali et al. (2013) is very rich in Sr (100 ppm) compared to other samples. Better concordance was obtained using the average composition of Sr from Middle Atlas lherzolites (44 ppm).

Early experimental studies on nephelinite petrogenesis demonstrated that lherzolite is a likely source for these magmas (Green, 1970). The lherzolite should be enriched in incompatible trace elements compared to the pyrolite, hydrated or carbonated, and partial melting degrees should be low (<5%) (Frey et al., 1978; Green, 1970). Partial melting experiments on mantle pyroxenite (e.g., Hirschmann et al., 2003; Kogiso et al., 2003) do not produce nephelinitic melts characterized by low Si (37–39 wt.% SiO_2) and high Ca (13–15 wt.%) as those from Saghro. The involvement of pyroxenite in the genesis of nephelinite magmas requires a complex two stages process: first, melting of a carbonated pyroxene-rich eclogite residue and formation of an alkali basalt and then, reaction of the latter with a peridotite (Mallik and Dasgupta, 2013). The presence of cognate carbonatite inclusions and carbonatite–apatite–Ba biotite domains in the Saghro nephelinites attest for the carbonated nature of the source (Berger et al., 2009) but the CO_2 content of the primitive Saghro nephelinites (between 1 and 1.5 wt.%; Berger et al., 2009; this study) is extremely low compared to those produced experimentally (17–19 wt.% CO_2 for a silica content of 38–39 wt.% SiO_2; Mallik and Dasgupta, 2013). Carbonated peridotite is a likely source for such Si-undersaturated alkaline magmas according to experimental studies (Dasgupta et al., 2007; Hirose, 1997). Experimentally produced melts from carbonated peridotite have however lower Ti contents compared to Saghro nephelinites (~3 wt.% TiO_2). This can be overcome by considering low partial melting degrees. Indeed, the lowest partial melting degrees reached

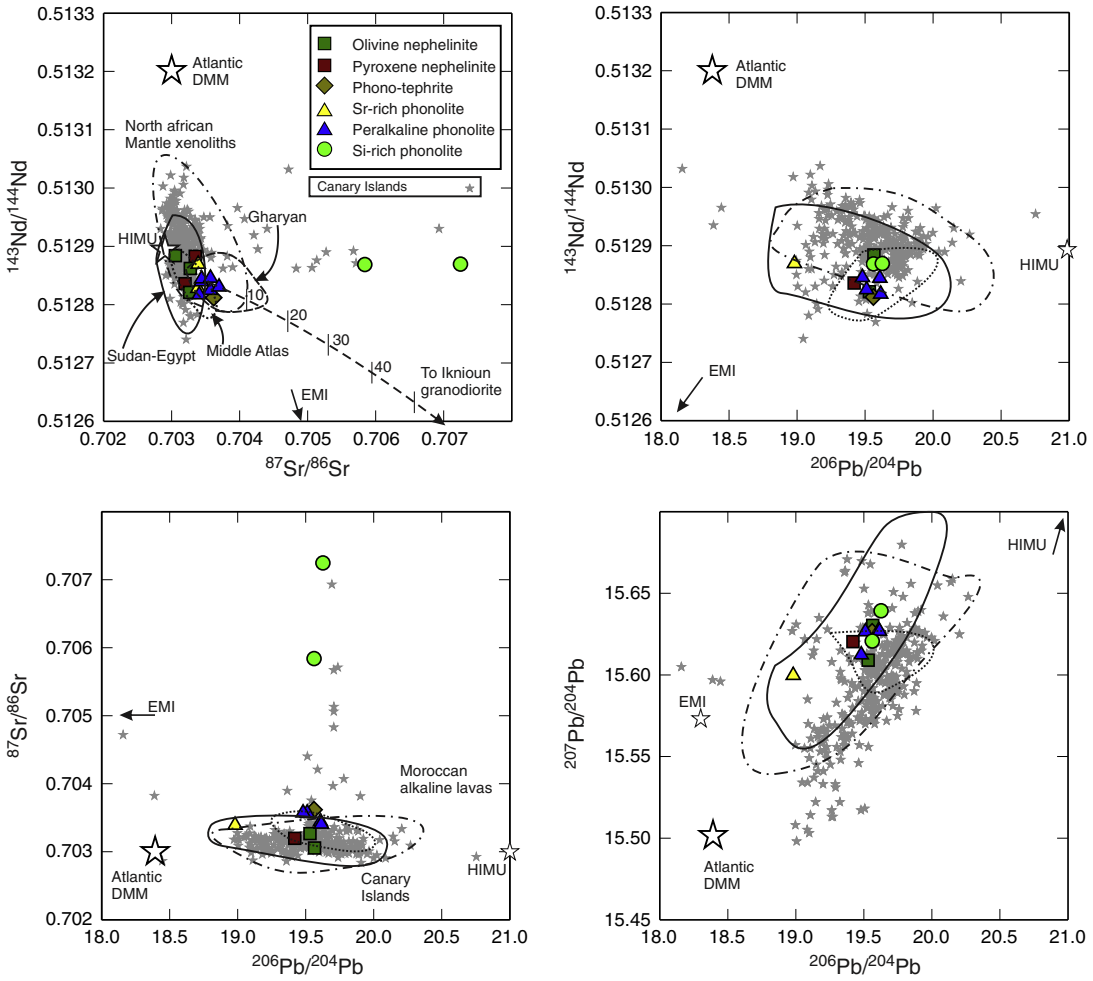

Fig. 6. Sr–Nd–Pb isotopic composition of Saghro lavas compared to other North African alkaline Cenozoic volcanic provinces and oceanic islands (Middle Atlas in Morocco; Canary Islands, Sudan and Egypt, Gharyan in Libya; data from Bosch et al., 2014; Duggen et al., 2009; Lucassen et al., 2008; Lustrino and Wilson, 2007; Lustrino et al., 2012). The DM end-member is the Atlantic MORB with the most depleted signature between latitudes 35° and 45°N (PetDB online database). The two end-members in the mixing curve of the Sr–Nd plot are the MIG phonolite and the Iknioun Neoproterozoic granodiorite (Errami et al., 2009). The mantle xenolith field comprises samples from the Middle Atlas, Algerian Hoggar and Libya (Beccaluva et al., 2007, 2008; Natali et al., 2013; Raffone et al., 2009).

in experiments are around 5% and extrapolation of experimental results toward lower values of partial melting points to higher Ti contents in the produced melt (3 wt.% TiO_2 for melt fractions around 1–2 wt.%; Dasgupta et al., 2007), corresponding to the Saghro values. These experiments however also produce melts with high CO_2 contents (10 wt.% for silica contents around 35–40 wt.%) compared to the mass balance estimations for the Saghro primitive nephelinite melt. According to Green (1970) the presence of minor amounts of water is required to produce nephelinites from a lherzolite source. In the case of Saghro lavas, amphibole is rare and only a few grains of kaersutite xenocrysts have been observed in the phonotephrite, indicating that water played a very minor role in the formation of nephelinites. As a conclusion, the data presented in this paper support a LREE-rich lherzolite lying in the spinel stability field and above the garnet stability domain as a source for primitive Saghro nephelinites. The presence of co-magmatic igneous carbonates in nephelinites and experimental evidences attests for the presence of CO_2 during melting, either as a free component or as carbonates in the source lherzolite.

7.2. Metasomatism and uplift of shallow mantle as trigger of Saghro volcanism

Partial melting simulation suggests that the source of nephelinite is a LREE-rich garnet-free, spinel lherzolite. Such mantle rocks, found as xenolith in Middle Atlas volcanoes has been formed by interaction with a metasomatic agent that is either a carbonatitic or a nephelinitic melt (Natali et al., 2013; Raffone et al., 2009). The timing of this alkaline/carbonatitic metasomatic event has been constrained by isotopic studies on Middle Atlas xenoliths to be less than 200 Ma, probably around 20 Ma (Wittig et al., 2010).

Sr–Nd–Pb isotopic composition of Saghro nephelinites form a narrow range characterized by high $^{206}Pb/^{204}Pb$ and $^{207}Pb/^{204}Pb$ ratios (~19.5 and 15.60–15.63 respectively), high $^{143}Nd/^{144}Nd$ ratio (0.5128–0.5129) and low $^{87}Sr/^{86}Sr$ ratios (0.7030–0.7035). The highly radiogenic lead isotopic composition depicts the involvement of a HIMU component while the low Sr and high Nd isotopic ratios with high Ce/Pb and Nb/U (50 for both) for primitive lavas imply a depleted mantle component with a negligible influence of enriched mantle (EM) end-member (i.e., recycled continental crust; Hofmann, 1997). This signature is typical of the sub-continental North African mantle and nearby oceanic islands sampled by Cenozoic alkaline lavas including the Middle Atlas and the Canary Islands (especially the Mio-Pliocene Gran Canaria nephelinites; Berger et al., 2010; Bosch et al., 2014; Bouabdellah et al., 2010; Duggen et al., 2009; Hoernle and Schmincke, 1993), nephelinites from Hoggar (Allègre et al., 1981) and the Eastern North African volcanism (Sudan–Egypt, Lucassen et al., 2008; Fig. 6). In the oceanic areas (Canaries), these characteristics are interpreted as evidences for a deep mantle plume rising to the lithosphere (Hoernle

Table 2
Sr–Nd–Pb isotopic composition of Saghro lavas.

	$^{87}Rb/^{86}Sr$	$\pm 2\sigma$	$^{87}Sr/^{86}Sr$	$\pm 2\sigma$	$^{87}Sr/^{86}Sr_i$	$^{147}Sm/^{144}Nd$	$\pm 2\sigma$	$^{143}Nd/^{144}Nd$	$\pm 2\sigma$	$^{143}Nd/^{144}Nd_i$	eNd	$^{208}Pb/^{204}Pb$	$\pm 2\sigma$	$^{207}Pb/^{204}Pb$	$\pm 2\sigma$	$^{206}Pb/^{204}Pb$	$\pm 2\sigma$	$^{208}Pb/^{204}Pb$	$^{207}Pb/^{204}Pb$	$^{206}Pb/^{204}Pb$
	Measured		Measured			Measured		Measured		5 Ma	5 Ma	Measured		Measured		Measured		5 Ma	5 Ma	5 Ma
Nephelinites																				
TAF	0.067	0.004	0.703277	0.000008	0.703273	0.0961	0.0019	0.512862	0.000012	0.512859	4.43									
TAB	0.141	0.008	0.703353	0.000007	0.703343	0.1004	0.0020	0.512883	0.000010	0.512880	4.84									
FN	0.112	0.007	0.703060	0.000007	0.703052	0.1067	0.0021	0.512884	0.000011	0.512881	4.86	39.1814	0.0032	15.6304	0.0012	19.5648	0.0014	39.181	15.630	19.565
TL	0.069	0.004	0.703270	0.000008	0.703265	0.0969	0.0019	0.512821	0.000008	0.512818	3.63	39.3058	0.0027	15.6091	0.0010	19.5321	0.0014	39.305	15.609	19.532
FS	0.052	0.003	0.703199	0.000010	0.703195	0.1049	0.0021	0.512836	0.000008	0.512833	3.92	39.1146	0.0030	15.6204	0.0010	19.4195	0.0012	39.114	15.620	19.419
Phono-tephrite																				
AS	0.293	0.017	0.703631	0.000008	0.703610	0.0929	0.0019	0.512812	0.000013	0.512809	3.46	39.3452	0.0022	15.6264	0.0008	19.5607	0.0013	39.345	15.626	19.561
Sr-rich phonolites																				
TO	0.187	0.011	0.703398	0.000010	0.703385	0.0927	0.0019	0.512869	0.000011	0.512866	4.58	38.7146	0.0036	15.5997	0.0013	18.9804	0.0016	38.714	15.600	18.980
OUL	0.170	0.010	0.703393	0.000007	0.703381	0.0882	0.0018	0.512828	0.000009	0.512825	3.78									
Peralkaline phonolites																				
TABS	1.130	0.066	0.703746	0.000010	0.703666	0.0718	0.0014	0.512830	0.000010	0.512828	3.83									
TG	0.424	0.025	0.703455	0.000010	0.703425	0.0922	0.0018	0.512839	0.000010	0.512836	3.99									
AZLOU	0.739	0.043	0.703602	0.000010	0.703550	0.0792	0.0016	0.512825	0.000009	0.512822	3.72	39.3181	0.0029	15.6265	0.0011	19.5117	0.0015	39.318	15.626	19.512
MIG	1.720	0.100	0.703645	0.000008	0.703523	0.0834	0.0017	0.512845	0.000007	0.512843	4.12	39.2511	0.0024	15.6123	0.0009	19.4804	0.0011	39.251	15.612	19.480
TIM	0.506	0.029	0.703462	0.000008	0.703426	0.0884	0.0018	0.512844	0.000010	0.512841	4.09	39.3570	0.0035	15.6272	0.0012	19.6085	0.0015	39.357	15.627	19.608
SAR	0.821	0.048	0.703441	0.000011	0.703383	0.0879	0.0018	0.512817	0.000012	0.512814	3.56	39.3729	0.0022	15.6267	0.0009	19.6148	0.0009	39.372	15.627	19.615
Si-rich phonolites																				
IK	8.327	0.483	0.706194	0.000008	0.705603	0.1018	0.0020	0.512869	0.000031	0.512865	4.56	39.3277	0.0017	15.6208	0.0006	19.5607	0.0008	39.327	15.621	19.561
ELB	6.603	0.383	0.707526	0.000007	0.707057	0.0698	0.0014	0.512869	0.000011	0.512867	4.59	39.3555	0.0030	15.6393	0.0010	19.6266	0.0015	39.355	15.639	19.626

Table 3
Summary of LA-ICP-MS data for minerals in equilibrium with their bulk sample composition.

ppm	Clinopyroxene						Titanite				Sanidine			
	FS	n = 5	TIM	n = 4	TO	n = 6	TO	n = 8	BAG	n = 6	IK	n = 4	BAG	n = 4
	Mean	Sigma (%)	Mean	Sigma (%)	Mean	Sigma (%)	Mean	Sigma (%)	Mean	Sigma (%)	Mean	Sigma (%)	Mean	Sigma (%)
Rb							1.2	21			107	33	151	27
Sr	266	13	642	51	1086	8	2086	8	1031	3	248	21	1962	31
Zr	169	17	366	38	332	1	1856	11	2103	17				
Nb	3.1	20	12.5	74	3.9	7	3810	5	5970	24				
Ba	5.0	12	7.8	92			13.4	14	14.2	22	51	24	3989	48
La	9.8	9	33	52	25	2	1403	6	1343	11				
Ce	26	9	64	34	46	4	2570	5	2930	13				
Nd	27	6	43	21	20	5	1233	7	1386	6				
Sm	7.1	5	9.3	24	4.0	17	207	9	240	9				
Eu	2.3	6	2.9	23	1.3	23	60	8	68	4				
Gd	5.8	9	7.6	20	3.5	28	149	8	164	8				
Dy	3.8	7	5.4	13	3.0	5	110	7	122	1				
Er	1.6	11	2.7	13	1.8	5	46	9	47	6				
Yb	0.8	9	2.0	27	2.1	12	26	7	27	4				
Hf	5.6	17	9.6	18	6.6	3	38	9	49	16				
Ta	0.4	36	0.9	25	0.3	9	216	8	295	26				

and Schmincke, 1993) inducing a mix of deep HIMU components with shallow DM asthenosphere and EM lithosphere (Gurenko et al., 2010). In detail, the Canary Island lavas have slightly higher radiogenic $^{143}Nd/^{144}Nd$ and lower $^{207}Pb/^{204}Pb$ ratios compared to Saghro lavas, attesting for slightly different source compositions. In continental areas, no low velocity anomalies are preserved below 200 km depth under the North African Cenozoic volcanic fields (Liégeois et al., 2005), this does not support a mantle plume origin for volcanism. Lateral horizontal propagation of the Canary mantle plume under the Atlasic lithospheric corridor has been proposed to explain the isotopic compositional similarities between Middle Atlas and Canaries (Duggen et al., 2009) but it does not fit to the Cenozoic geological evolution of the Atlasic belts (Berger et al., 2010) and it does not explain the presence of similar source composition under Algerian Hoggar and East Africa. Instead, the Hoggar, Sudan–Egypt, Lybian, Middle Atlas and Anti-Atlas volcanic rocks are lying upon the former Variscan and/or Pan-African belts that have been uplifted during the Cenozoic (Berger et al., 2010; Liégeois et al., 2005; Lucassen et al., 2008; Rougier et al., 2013). The Pan-African orogenic event was characterized by oceanic and continental subductions, formation and accretion of arcs that produced intense metasomatism of the lithospheric mantle (Caby, 2003; Thomas et al., 2002). The HIMU component is often interpreted as pieces of altered subducted oceanic crust recycled into the deep convecting mantle (Stracke et al., 2003) or within the upper mantle (Bianchini et al., 2010). Lucassen et al. (2008) however pointed out that high-μ sources can be a fingerprint of Pan-African lithospheric mantle metasomatized during Neoproterozoic subductions and arc-forming events in northern Africa. Lustrino et al. (2012) also argue that Gharyan lavas with similar Sr–Nd isotopic signature than North Africa alkaline intraplate lavas are formed from shallow metasomatized mantle sources. Such mixed DM–HIMU signatures could thus reflect a shallow lithospheric source close to the asthenosphere–lithosphere boundary located around between 60 and 100 km depth below Saghro (Fig. 1, Missenard et al., 2006), consistently with the absence of garnet in the source of nephelinites. Petrological and isotopic data on mantle xenoliths collected in North African alkaline volcanics from the Middle Atlas (Natali et al., 2013; Raffone et al., 2009), Libya (Beccaluva et al., 2008) and Hoggar (Beccaluva et al., 2007) show that the underlying mantle share similar isotopic signatures than lavas: $^{143}Nd/^{144}Nd$: 0.5128–0.5130, $^{87}Sr/^{86}Sr$: 0.7028–0.7036 and $^{206}Pb/^{204}Pb$: 19.0–20.5. These xenoliths record metasomatism, either by alkaline melts or carbonatitic fluids and also record local upwelling of the uppermost astenospheric mantle leading to thermal rejuvenation of the lithosphere. The influence of a deep mantle plume on the origin of Cenozoic North African volcanism is neither supported by studies on these real mantle samples, nor by geological, tectonic and geochronological investigations of the Atlasic areas (see Berger et al., 2010). The mantle below Saghro as seen through the trace element and isotopic composition of nephelinites probably records two metasomatic events: interaction with carbonatitic and alkaline silicated melts during the Cenozoic and old Late Precambrian event related to the Pan-African orogeny.

7.3. Calculation of the impact of accessory phases in trace elements evolutionary trends

Despite a small silica gap between 44 and 52 wt.% SiO_2 (Berger et al., 2009; Berrahma et al., 1993), the nephelinites and phonolites of Saghro display linear and curved evolution trends in diagrams

Table 4
Partition coefficients used for fractional crystallization calculations.

	Sr	Zr	Nb	Ce	Nd	Sm	Dy	Yb	Hf	Ta
Olivine/nehelinite[a]	0.02	0.06		0.03	0.03	0.03	0.03	0.03	0.04	0.03
Cpx/nephelinite[b]	0.14	0.59	0.02	0.11	0.30	0.46	0.54	0.33	0.99	0.05
Cpx/phonolite[b]	0.42	0.85	0.02	0.31	0.53	0.71	1.00	1.05	1.07	0.04
Titanite/phonolite[b]	0.8	5.6	19.5	21.3	37.3	42.4	35.2	12.0	9.0	36.5
Nepheline/melt[a]	0.02	0	0	0	0	0	0	0	0	0
Apatite/melt[a]	14	0.0	0.0	12.0	14.0	14.6	14.0	8.1	0.0	0
Perovskite/melt[a]	4	1.3	70	22	25	27	14	10	1.3	70
Melilite/melt[a]	7	0.4	0	0.6	0.7	0.77	0.52	0.3	0.4	0
Sanidine/melt[a]	2	0.13	0.08	0.24	0.2	0.16	0.12	0.1	0.13	0.08
Carbonatite/nephelinite[b]	3	3.0	3	3	3	3	3	3	3	0.5

[a] Literature data.
[b] This study.

involving trace elements. Considering the similar isotopic composition between nephelinites and phonolites (except for a slight shift in Sr isotopic composition) and the similar K–Ar ages (Berrahma et al., 1993), the compositional evolution can be simulated using the fractional crystallization equation:

$$C_l = C_0 \times (1-\mathrm{F})^{(\overline{D}-1)}$$

where C_l is the concentration in the evolved liquid, C_0 the concentration in the parental liquid, F is the fraction of remaining liquid and $\overline{D}$ is the bulk partition coefficient defined as follows:

$$\overline{D} = \sum_{i=1}^{n} X_i \times D_i$$

where X_i is the weight fraction of phase i and D_i is the partition coefficient of phase i for the considered element.

Partition coefficient used for clinopyroxene, feldspar and titanite is the mineral/bulk-rock ratios calculated with data presented in this paper. Equilibrium partition coefficient determined with experimental studies is indeed strongly dependent of melt composition, especially for clinopyroxene and titanite (Prowatke and Klemme, 2005), and strongly variable (see Olin and Wolff, 2012; Prowatke and Klemme, 2005). Additionally, data for the elements of interest in this study such as Nb, Ta or Hf are often missing in published datasets. By choosing mineral/bulk rock coefficient in this study with a control on texture and chemistry for equilibrium, we use coefficients that are appropriate for the bulk composition even though phyric samples do not always represent the composition of a pure melt. REE concentration in feldspar was below detection limits, the values of Villemant et al. (1981) determined in alkaline series were thus selected for this study (Table 4). Different values were used for clinopyroxene/nephelinite and for clinopyroxene/phonolite coefficients, according to LA-ICP-MS data. Data for perovskite and melilite are scarce and also strongly variable. Recent experiments have determined perovskite/melt partition coefficient in kimberlitic systems (Chakhmouradian et al., 2013) but the only source for perovskite/nephelinite trace element coefficient is from Onuma et al. (1981). The concentrations determined with electronic microprobe for Sr, Zr and Nb in these minerals were used to compute partition coefficient. Values for Ta and Hf were assumed to be equal to those for Nb and Zr, respectively. For apatite, the coefficient determined with microprobe data is around 8–15 for Sr and 7–17 for Ce, the data (run 61B) from Prowatke and Klemme (2006) were used because published Ce coefficient are within the range determined in this study (Table 4). Major element modeling (Berger et al., 2009) resulted in the production of igneous carbonates at the first stages of differentiation probably by unmixing and subsequent crystallization of a carbonatitic melt, a carbonate component was included in the calculation and the mineral/bulk rock coefficients are the ratio between composition of Saghro carbonatite (Ibhi et al., 2002) and the host nephelinite (FS, this study).

The main source of uncertainty in this calculation consequently arises from the poorly constrained partition coefficients. For simplicity,

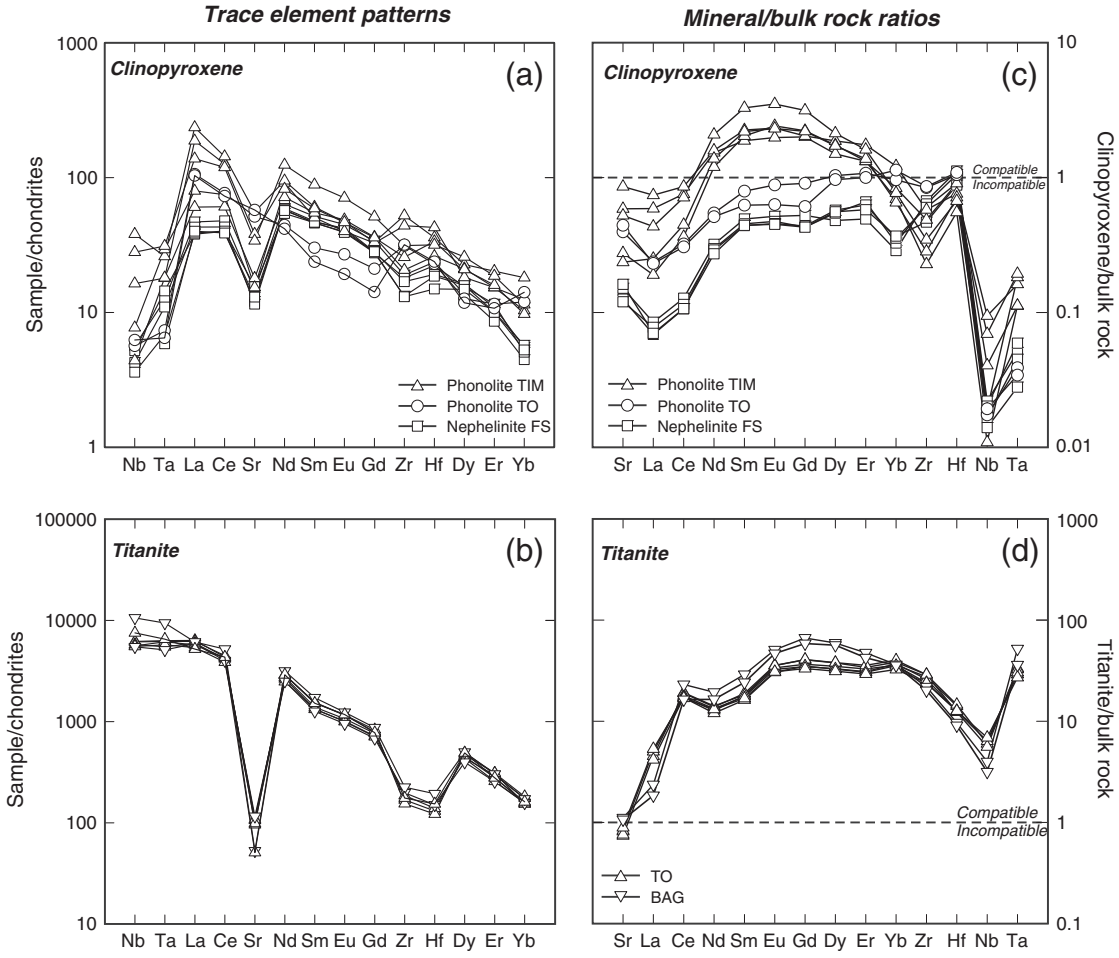

Fig. 7. Plots of trace element concentration and distribution in clinopyroxene and titanite from Saghro. Chondrite-normalized trace element patterns of clinopyroxene (a) and titanite (b). Mineral/bulk rock ratios of clinopyroxene (c) and titanite (d).
Normalization values from McDonough and Sun (1995).

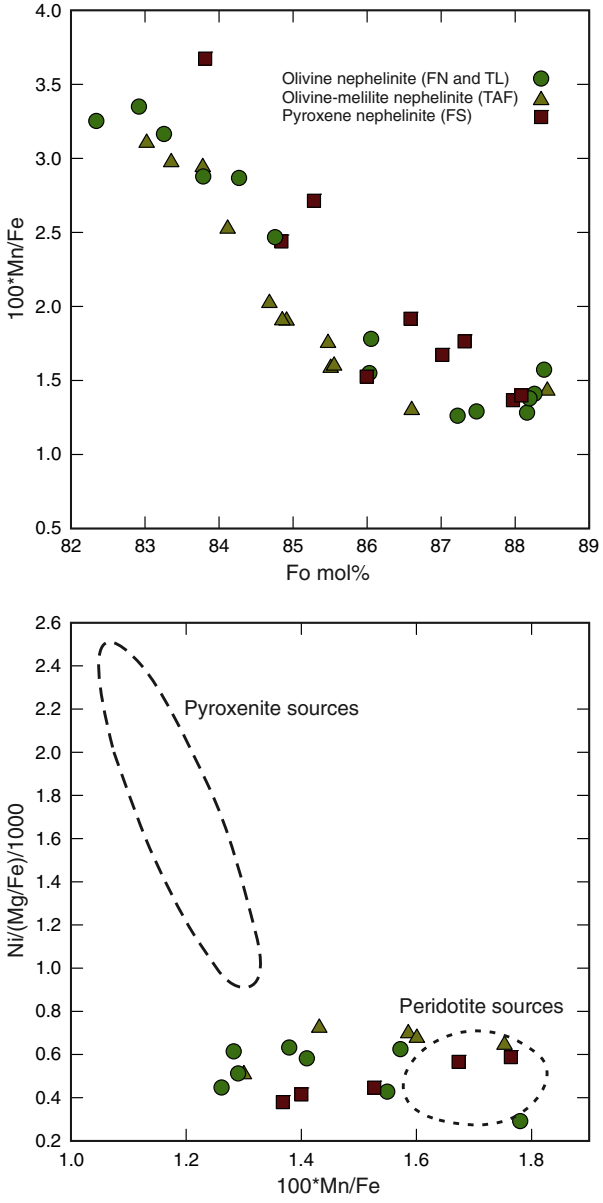

Fig. 8. Minor element contents of olivine used to estimate the nature of the mantle source. Comparison fields are from Herzberg (2011).

the partition coefficients were taken as constant for varying Si contents (except for clinopyroxene were two different set of values were used for nephelinites and phonolites) even if this is probably far from reality where partition coefficients vary in function of melt polymerization degree, mineral composition, temperature, pressure and oxygen fugacity. Estimation of the proportion of fractionating minerals based on major-elements gave good results for major minerals such as olivine, clinopyroxene, feldspar and nepheline but it is less sensitive for accessory phases (Berger et al., 2009). On the other hand, because accessory phases such as titanite and apatite have mineral/melt partition coefficient for trace elements that are 10 to 1000 times higher than for the more abundant silicates, they have a high weight in calculations based on trace elements. As a consequence, these calculations do not give good results for the estimation of the proportion of major silicate phases as they have a very low weight in the calculation. Fractional crystallization calculations using major elements have demonstrated that the crystallizing assemblages evolved from wehrlite–pyroxenites to agpaitic nepheline syenites during differentiation of the Saghro magmas (Berger et al., 2009). These cumulates are typical of ultramafic–alkaline–carbonatite complexes (Downes et al., 2005).

A trend was visually fitted for each modeled element and 9 steps were fixed on this trend (white crosses on Fig. 3, including the most primitive liquid). The estimation of the weight fraction for each phase and F at each step for all elements was made while fitting the model to the trends by successive iteration (see results on Fig. 10). The difference between the visually chosen steps (dark crosses) and the calculated ones (white crosses) can be visualized on Fig. 3. The results of fractional crystallization calculations are presented in Table 6 and Figs. 3, 4 and 10.

The continuous decrease in LREE, MREE and Sr is controlled by the crystallization of apatite. About 10–12 wt.% of apatite is fractionated in the solids during the three first steps (1-F: ~0.1). The stagnant Ce and Sr values for silica contents between 45 and 50 wt.% are accommodated by lower proportion of apatite in fractionated solids, 2–4 wt.% until the last steps of differentiation. Iterations did not satisfactorily converge for Sr between 47 and 49 wt.% SiO_2 in melt and for Ce between 51 and 55 wt.% SiO_2. The results are however still in the range of analytical results. Fractionation of perovskite (2 to 0.5 wt.%) at low silica contents (Fig. 10) controls the decrease observed for HREE and Y. As perovskite stop crystallizing, these elements became incompatible (47–55 wt.% SiO_2). Titanite starts crystallizing when the melt reaches 47 wt.% SiO_2 (Fig. 10). This not only corresponds to the shift in Ta contents but also to the formation of melts with concave downward patterns (with low MREE/LREE and MREE/HREE ratios). Unlike LREE and Sr, MREEs do not show stagnant values at intermediate composition. Titanite preferentially incorporates MREE over LREE and this leads to a continuous compatible behavior for MREE. The drastic change in Nb/Ta and Zr/Hf ratios observed at intermediate composition is also explained by the onset of titanite crystallization (Figs. 3, 4 and 10) as it has the strongest affinity for Ta over Nb and for Hf over Zr. The calculation also produced fractionation of carbonates at the first steps of differentiation (about 10 wt.% in the two first fractionated solids, Fig. 10). This, together with fractionation of apatite, explain the strong decrease in LREE observed for melt SiO_2 contents below 43 wt.%, the same results were obtained with independent fractional crystallization calculation based on major elements (Berger et al., 2009). Melilite is present in the fractionated solid at 43 and 45 wt.% SiO_2 but removing melilite from the calculation does not significantly change the goodness of the fit.

Phosphorus can be used to control if the total amount of apatite produced with the trace elements based calculations is significant. On 100 g of starting material, 4.3 g of apatite has been fractionated. Considering 45 wt.% of P_2O_5 in apatite, this leads to a total consumed contents of 1.8 wt.% P_2O_5. The most P-rich primitive nephelinite (taken as the starting composition for calculations) has 2.0 wt.% P_2O_5, which is in good agreement with the calculated values. If the computed extracted carbonatite fraction is reintroduced into the primitive nephelinite, a CO_2 content of 0.9 wt.% is obtained for the primitive melt using results from trace element calculations and 1.6 wt.% using major element calculation results (Berger et al., 2009).

7.4. Fractional crystallization impact on Nb/Ta and Zr/Hf ratios

The Nb/Ta ratio evolves from 18.1–18.8 in the nephelinites (with the evolved pyroxene nephelinite TAB 3 having already a fractionated ratio of 20.4) to 70 in the peralkaline phonolites, eventually dropping down to 38–55 in the two most differentiated Si-rich phonolites (Figs. 4 and 11). Zr/Hf ratios are more scattered in primitive nephelinites (42–56); it increases to 64–82 for peralkaline phonolites and also drops to 60–70 for the most differentiated Si-rich phonolites (Figs. 4 and 11). Increasing Nb/Ta and Zr/Hf ratios during differentiation also characterize the Eocene Tamazert sub-volcanic alkaline-carbonatitic complex in the High-Atlas (Marks et al., 2008). In other alkaline volcanic series showing lower Si-undersaturation, Nb/Ta and Zr/Hf do not increase and increase only slightly during differentiation (for example, Gharyan lavas in Libya,

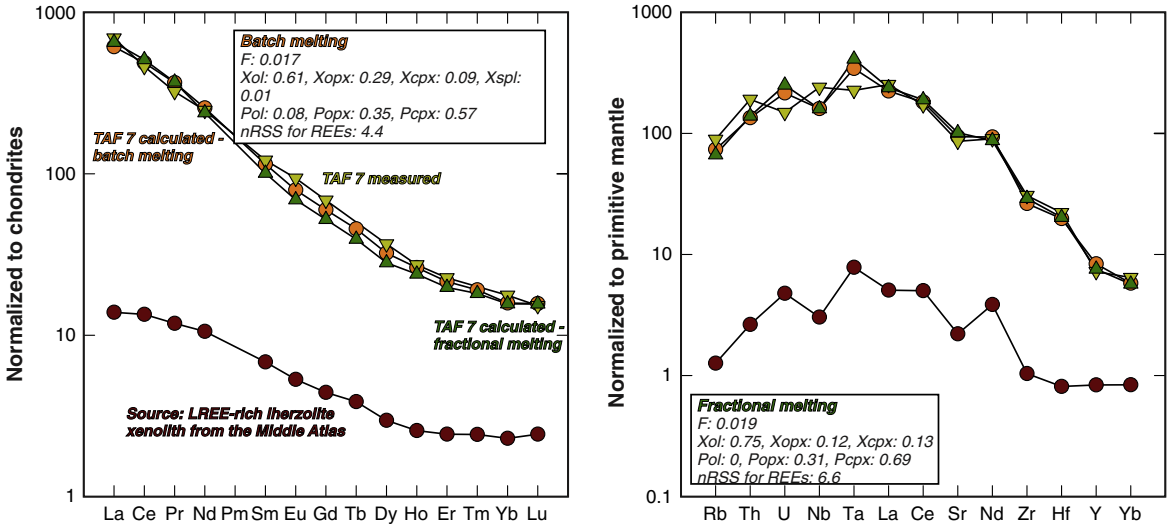

Fig. 9. Results of non-modal batch and fractional melting calculations using the LREE rich lherzolite composition of Natali et al. (2013) (Middle Atlas xenolith). The most LREE-rich primitive Saghro nephelinite is best reproduced using batch melting equation for a liquid fraction of 1.7 wt.%.
Normalization values from McDonough and Sun (1995).

Lustrino et al., 2012; Fig. 4). Nb/Ta ratios in Saghro nephelinites are slightly sub-chondritic (19.9) while Zr/Hf is super-chondritic (>34.3) and above most OIB (Pfander et al., 2007). This ratio is not significantly different between primitive and evolved nephelinites while Nb and Ta concentrations are variable (130–190 and 6.8–10.3 ppm respectively; Fig. 11). By contrast the Zr/Hf ratio is positively correlated to both Zr and Hf concentrations in nephelinites, which are in turn correlated to the bulk MgO content of nephelinites (Fig. 11). Fractionation of olivine–clinopyroxene assemblages, with the latter mineral phase having moderate partition coefficients for both Zr and Hf (0.46–0.67 and 0.88–1.12) and low D_{Zr}/D_{Hf} (0.53–0.66), can explain the early increase in Zr/Hf ratios. Clinopyroxene can also fractionate Nb from Ta (D_{Nb}/D_{Ta}: 0.34–0.50) but these elements are strongly incompatible in clinopyroxene (D < 0.05). Therefore, crystallization of clinopyroxene only traps a small fraction of Nb and Ta from the bulk system, leading to an increase of concentrations in the melt, but not to detectable variation of the Nb/Ta ratio in the remaining liquid.

A strong increase of both ratios occurs when titanite starts crystallizing (Fig. 4). Titanite is characterized by low D_{Nb}/D_{Ta} and D_{Zr}/D_{Hf} (0.45–0.62 and 0.59–0.79, respectively) and very high partition coefficient for Ta (27–52) and Hf (3–20; this study; Wolff, 1984;

Table 5
results of batch and fractional melting calculations.

Batch melting	Prop in source	Prop in melt
Ol	0.61	0.08
Opx	0.29	0.35
Cpx	0.09	0.57
Spl	0.01	0.00
nRSS for REE	4.4	
F	0.017 (=1.7%)	

	Rb	Sr	Y	Zr	Nb	La	Ce	Pr	Nd	Sm	Eu	Gd	Dy	Ho	Er	Yb	Lu	Hf	Ta	Th	U
Source	0.76	44	3.6	10.9	2	3.29	8.26	1.1	4.83	1.01	0.3	0.88	0.73	0.14	0.39	0.37	0.06	0.23	0.29	0.21	0.11
Calc liq	44.2	1871	36.0	277	105	145	299	34.1	117	17.0	4.47	11.9	7.94	1.43	3.44	2.55	0.39	5.61	12.7	10.7	4.96
Meas liq	53.7	1716	31.1	322	158	164	283	30.0	113	17.9	5.28	13.7	9.05	1.49	3.63	2.85	0.37	6.28	8.39	15.2	3.43
nSR	1.6	14.0	0.8	6.3	17.5	2.3	0.9	0.6	0.1	0.1	0.1	0.2	0.1	0.0	0.0	0.0	0.0	0.1	2.2	1.3	0.7

Fractional melting	Prop in source	Prop in melt
Ol	0.76	0.00
Opx	0.12	0.31
Cpx	0.12	0.69
Spl	0.00	0.00
nRSS for REE	6.2	
F	0.019 (=1.9%)	

	Rb	Sr	Y	Zr	Nb	La	Ce	Pr	Nd	Sm	Eu	Gd	Dy	Ho	Er	Yb	Lu	Hf	Ta	Th	U
Source	0.76	44	3.6	10.9	2	3.29	8.26	1.1	4.83	1.01	0.3	0.88	0.73	0.14	0.39	0.37	0.06	0.23	0.29	0.21	0.11
Calc liq	40.0	2019	32.6	306	105	155	312	34.4	109	14.9	3.89	10.4	6.92	1.31	3.17	2.52	0.38	5.73	15.2	11.0	5.77
Meas liq	53.7	1716	31.1	322	158	164	283	30.0	113	17.9	5.28	13.7	9.05	1.49	3.63	2.85	0.37	6.28	8.39	15.2	3.43
nSR	3.5	53.5	0.1	0.9	17.7	0.6	3.0	0.6	0.1	0.5	0.4	0.8	0.5	0.0	0.1	0.0	0.0	0.0	5.6	1.1	1.6

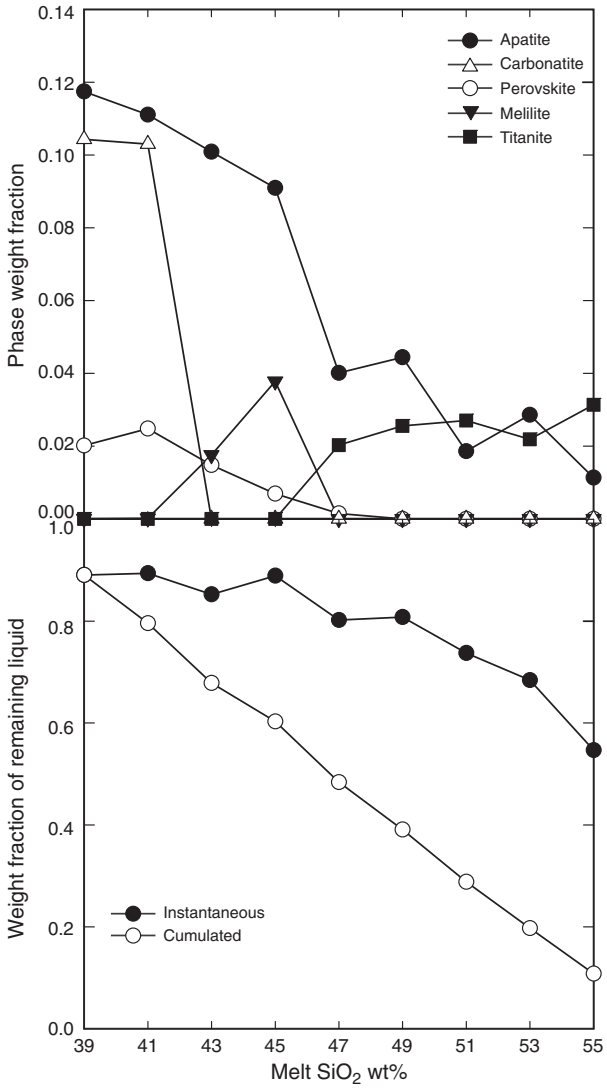

Fig. 10. Results of fractional crystallization simulation. See text for explanations.

Prowatke and Klemme, 2005). Crystallization of more than 2 to 4 wt.% of titanite in the fractionated solid leads Ta to behave like a slightly compatible element during differentiation while Nb, Zr, and Hf still behave like incompatible elements when integrated in the bulk solid ($D^{titanite/melt} < 25$ for Zr, Nb and Hf). The results of fractional crystallization simulation show that titanite crystallized at a proportion of 2–3 wt.% in the fractionated solid; such values explain the stagnation of Ta during differentiation from nephelinites (7–10 ppm) to phonolites (4–12 ppm).

In SiO_2 vs. Nb/Ta and SiO_2 vs. Zr/Hf plots (Fig. 4), the peralkaline phonolites (which are also the richest samples in Nb and Zr, Fig. 11) show increasing ratios with increasing silica (up to 70 and 80 respectively) but the two most differentiated (i.e., Si-rich, LREE-, Sr-, P-poor) phonolites show lower ratios (47–54 and 62–70, respectively). Late stage evolution in the phonolites is marked by the crystallization of a variety of minerals (hainite, lorenzenite, eudialyte-group minerals) in which Nb and Zr can be a major element (up to 1.5 wt.% Nb_2O_5 and 4.4 wt.% ZrO_2; Berger et al., 2009). They are accessory phases (<0.5 vol.%) but their fractionation in agpaitic nepheline syenites in the magma chamber can eventually lead to a drop of Nb and Zr contents in melt with a decrease in Nb/Ta and Zr/Hf ratios (this cannot be confirmed as Hf nor Ta have been measured in these phases).

The Sr isotopic ratio of the two Si-rich phonolites is higher than peralkaline phonolites. An origin of the peculiar trace elements and isotopic characteristics of the two phonolites by contamination by the surrounding rocks (the Iknioun granodiorite) is unlikely. Hence, it would require 40 to 70% of contaminant in the mix that would also induce a shift of Nd isotopic ratio (Fig. 6) compared to peralkaline phonolites and in most elements including silica, which is not observed. Knowing the mobile behavior of Sr, the isotopic shift could be due to late magmatic fluid–rock interactions between the cooling body of phonolite and the surrounding Neoproterozoic rocks with high $^{87}Sr/^{86}Sr$. Peralkaline fluids are rich in halogens and these elements are known to mobilize HFSE and more particularly Nb, Ta, Zr and Hf during complex late- to post-igneous hydrothermal alteration (Salvi and Williams-Jones, 2006). One other possibility for the final stage decrease in both Nb/Ta and Zr/Hf ratios is that these fluids could have fractionated the two geochemical pairs.

Although no quantitative constraints can be obtained for the late stage behavior of HFSE, it is probable that fractionation of agpaitic assemblages from the peralkaline phonolites and/or the action of late

Table 6
Calculated concentrations and mineral proportions using fractionation crystallization inversion.

Calculated trace-element contents for each step

SiO_2	Sr	Zr	Nb	Ce	Nd	Sm	Dy	Yb	Hf	Ta
39	1850	273	185	243	97	14.6	7.4	2.6	5.4	8.9
41	1650	299	165	191	74	12.3	5.8	2.1	6.1	7.8
43	1501	350	165	160	62	10.3	5.1	1.9	7.4	7.8
45	1403	392	174	155	59	9.8	5.0	1.8	7.8	7.9
47	1534	486	195	157	52	8.5	4.5	1.8	8.9	7.4
49	1511	600	223	152	46	7.2	4.0	1.9	9.1	7.1
51	1300	762	263	159	41	6.0	3.9	2.3	10.5	7.0
53	903	1007	340	135	35	5.0	3.5	2.6	13.7	7.6
55	600	1551	415	121	24	3.4	2.9	3.6	21.1	6.7

Mineral portion and degree of fractionation at each step

SiO_2	Apatite	Perovskite	Melilite	Carbonatite	Titanite	F
39	0.12	0.02		0.10		0.89
41	0.11	0.02		0.10		0.89
43	0.10	0.01	0.02			0.85
45	0.09	0.01	0.04			0.89
47	0.04				0.02	0.80
49	0.04				0.03	0.81
51	0.02				0.03	0.74
53	0.03				0.02	0.68
55	0.01				0.03	0.55

stage peralkaline fluids induced a fractionation of the two geochemical twins, namely Zr–Hf and Nb–Ta and a decrease of Nb/Ta and Zr/Hf ratios in the most evolved Si-rich phonolites.

7.5. Possible remelting of nephelinitic rocks

Some geochemical features of phonolites cannot be explained by fractional crystallization only. The two Sr-rich, non-peralkaline phonolites (TO and OUL) are intermediate between nephelinites and phonolites for most elements (Si, Rb, REE Nb, Ta, Zr, Hf, Th) despite their very low Mg contents compared to the most primitive peralkaline phonolites (0.58–0.65 against 2.4 wt.% MgO respectively). They are however not lying on fractional crystallization trends for some elements such as Sr (2600–3000 ppm) and Ba (1800–2000 ppm) but also for Zr, Hf, and Yb although this is less pronounced than for Sr and Ba (Fig. 3). Compared to other phonolites, they are the only samples with $K_2O \geq Na_2O$ (in wt.%). One can argue that they represent primitive phonolite formed after fractionation of the nephelinitic magma but their very low Mg contents does not fit this hypothesis. Continuous fractionation of apatite should also lead to lower concentration of Sr in phonolites compared to nephelinites (but these two phonolites are richer in Sr compared to nephelinites). The lower Pb isotopic ratios in the Sr-rich phonolites cannot be explained by crustal contamination or by a different source for the parental magma, as they share the Sr and Nd isotopic compositions of the main group of peralkaline phonolites. Moreover, high Sr and Ba contents cannot be due to the assimilation of wall-rocks as the latter have low Sr and Ba contents (Errami et al., 2009). It can thus only be attributed to a late-stage alteration. The shift in some trace element content for the two Sr-rich phonolites is observed for mobile and immobile elements. Anomalous concentration in Sr and Ba and to a lower extent of Zr, Hf and Y coupled with a usual distribution of the other elements has to find their origin into an igneous process.

Remelting of solidified basic-ultrabasic alkaline magma in response to new inputs of primitive mantle-derived, high-temperature magmas in the crust have been invoked to explain the origin of some phonolites (Hay et al., 1995; Legendre et al., 2005). Remelting of H_2O- and CO_2-bearing sodic basic magma yielded silica-undersaturated intermediate magmas with K_2O contents close or above Na_2O (Hay et al., 1995; Legendre et al., 2005) and amphibole-rich residues. Amphibole has been found in millimeter-size hornblendite xenoliths in Saghro (Ibhi et al., 2002) and as corroded xenocrysts in the phonotephrite (Berger et al., 2009). Up to now, many experiments have been performed on

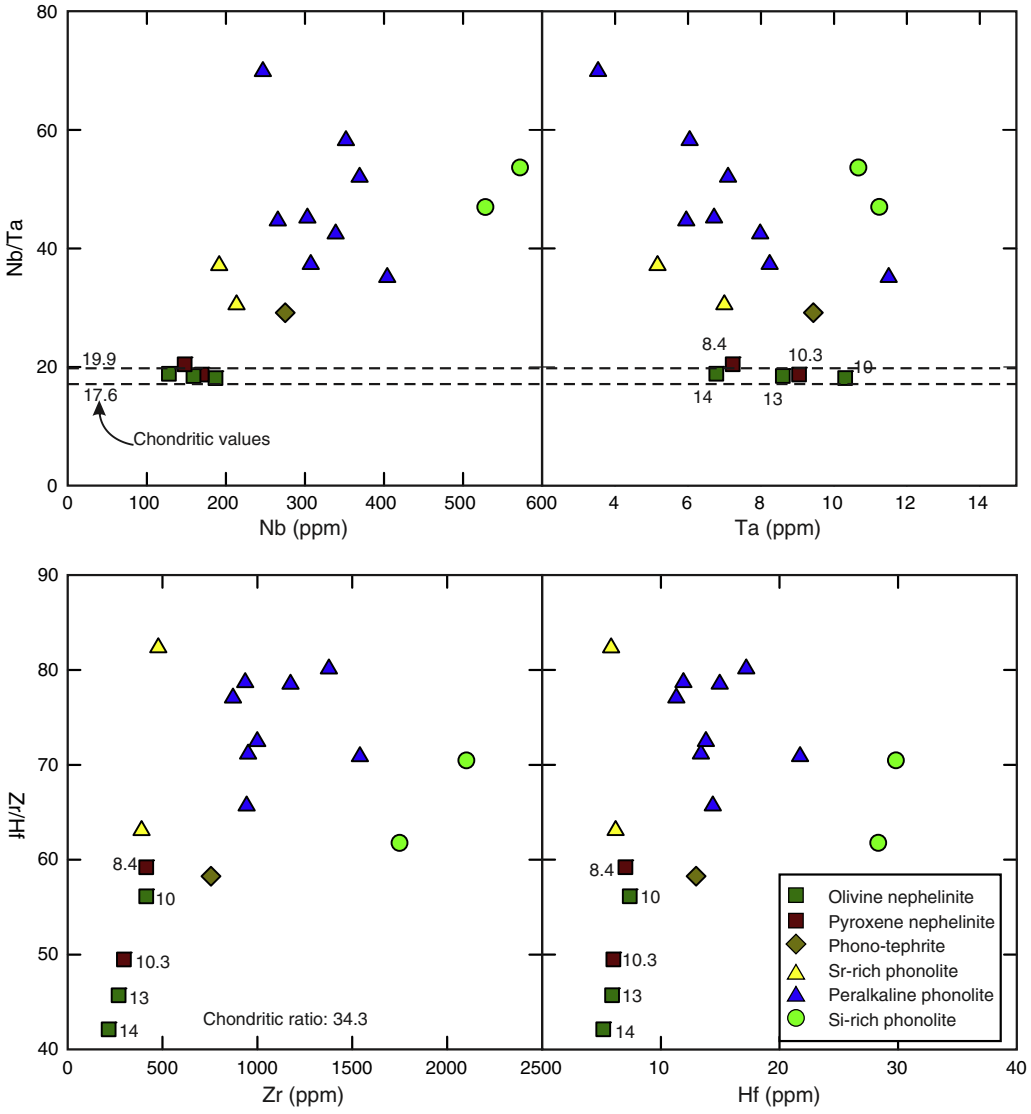

Fig. 11. Evolution of Nb/Ta and Zr/Hf ratios with concentration in Nb, Ta, Zr and Hf. The labels close to nephelinites are the MgO content of each sample. Chondritic values are from Pfander et al. (2007) and McDonough and Sun (1995).

trachytic basalt starting composition (45 wt.% SiO_2) producing a partial melt that is more silica-rich and less alkaline that the two Sr-rich phonolites from Saghro. On the other hand, Kaszuba and Wendlandt (2000) highlighted that melting of a more basic and alkali-rich basalt can lead to the production of phonolite. The experiments only deal with major element and the behavior of trace elements during partial melting of basic alkaline rocks has not been investigated. Legendre et al. (2005) showed that Sr and Ba behave like incompatible elements during partial melting of alkaline basaltic rocks, which can explain the elevated Sr and Ba contents of the Sr-rich phonolites. Although no qualitative constraints can be obtained on trace element budgets for partial melting of nephelinite, this hypothesis can explain the higher K/Na ratios of the Sr-rich phonolites and their Sr and Ba contents.

8. Conclusions

Mantle-derived primitive Cenozoic nephelinites in Saghro are partial melts from a carbonated LREE-rich spinel lherzolite. Their high incompatible element contents compared to other basic and ultrabasic magmas from the Circum Mediterranean province arise from a very low degree of partial melting, estimated at around 2% through inversion of trace element data, and the high incompatible element content of the metasomatized lherzolite source. Sr–Nd–Pb isotopic compositions are compatible with a mixed DM–HIMU signature close to FOZO. The HIMU component is here interpreted to originate from the shallow lithospheric mantle that kept traces of the Pan-African metasomatism, in agreement with other North African volcanic provinces.

Phonolites are linked to nephelinites by a fractional crystallization process. They show similar isotopic values, except for slightly more radiogenic signature in Sr that can be associated to hydrothermal alteration. Fractional crystallization calculations using published and newly determined mineral/bulk rock ratios show that the decrease of LREE, Sr and Ba with increasing differentiation is controlled by crystallization of large volume of apatite. Hf, Ta and MREE behave like moderately incompatible to compatible elements during differentiation while Nb, Zr and Th reach extremely high concentration in the most differentiated phonolites. This is explained by the fractionation of small amounts of titanite which has high partition coefficients for Ta, Hf and MREE compared to other trace elements. Nb/Ta and Zr/Hf ratios in volcanic rocks consequently increase with increasing silica content, reaching highly super-chondritic values, up to 70 and 80 respectively.

Titanite starts crystallizing when the magma reaches 45 SiO_2 wt.%, but the Zr/Hf ratios already increase from the most primitive to differentiated nephelinites. Clinopyroxene also fractionates Hf from Zr, leading to an early increase of Zr/Hf values. Low Zr/Hf and Nb/Ta ratios in the most differentiated Si-rich phonolites compared to less evolved peralkaline phonolites is tentatively explained by fractionation of volatile-rich agpaitic assemblages in the underlying magma chamber before the formation of the most evolved magmas. It is also supported by the decrease in peralkaline character with increasing silica content.

The Saghro nephelinites and phonolites represent a nice example of magma differentiation with uncommon fractionation trends for trace elements. It is the direct consequence of the partial melting mechanisms in the metasomatized mantle source that leads to the formation of volatile-rich Si-undersaturated magma. Crystallization of perovskite, apatite, titanite, carbonates and late stage Nb–Zr–REE rich sorosilicates induced decoupling of some trace elements generally characterized by similar geochemical behavior.

Supplementary data to this article can be found online at http://dx.doi.org/10.1016/j.lithos.2014.09.018.

Acknowledgments

Discussion with Mathieu Benoit (GET) and Daniel Demaiffe (ULB) led to some ideas presented in this paper. Viktor Sharygin shared some new observations on phonolites from Saghro that were used in this paper. We want to thank the local people from Saghro for their hospitality in sharing their home and food with us during fieldwork. G. Bianchini and an anonymous reviewer provided insightful comments that leaded to significant improvements of this manuscript.

Analytical appendix

Electron microprobe analysis of olivine

Olivine grains were analyzed with a CAMECA SX51 microprobe at UMons (Belgique). Operating conditions were 40 kV for the accelerating voltage and 40 nA for the current. Counting times were set at 30 s for peak and 30 s for background (15 s at each side of the peaks).

LA-ICP-MS analyses

Trace elements in minerals were collected with a UV Fisons laser probe coupled to a VG elemental Plasmaquad (PQ2 Turbo Plus) ICP-MS (Musée Royal de l'Afrique Centrale at Tervuren). The power of output beam is maximum (2 mJ/pulse) for a 10 Hz repetition rate of pulse, that is attenuated to obtain the required energy to get the appropriate crater size. The typical size of the crater is in the range 60 to 80 μm. Each sample and standard was ablated for 60 s, corresponding to 5 pulses of pre-ablation to clean the surface followed by 20 s of blank acquisition and 40 s with laser beam turned on. The raw data on each isotope peak were subtracted from the gas blanks and normalized to the ^{43}Ca or ^{29}Si signal and then compared to calibration lines. Calibration was done using NIST 610 synthetic standard. Typical accuracies and detection limits for this LA-ICP-MS system can be found in Féménias et al. (2003).

Bulk rock major and trace element data

Rock powders were mixed with a lithium tetraborate flux in proportion 1:6. The mix was heated at 1000 °C during 2 h and then dissolved in diluted nitric acid after cooling. For trace elements, final dilution factor is around 6000. Major elements were dosed by ICP-AES at Musée Royal de l'Afrique Centrale at Tervuren using a set of natural reference materials. Trace elements contents were determined by ICP-MS on a VG elemental Plasmaquad (PQ2 Turbo Plus) ICP-MS using artificial solution for calibration. Detailed analytical methods can be found in Liégeois et al. (2003).

Sr–Nd–Pb isotopic analysis

Sr and Nd were isolated using conventional ion-exchange chromatography techniques detailed in Pin et al. (1994). Isotopic composition was analyzed by TIMS on a VG sector 54 spectrometer owned by Musée Royal de l'Afrique Centrale at Tervuren (Belgium). Details on Sr–Nd isotopic analysis can be found in Liégeois et al. (2003). Pb was extracted following the method of Weis et al. (2006). It was analyzed on a Nu plasma MC-ICP-MS at Université Libre de Bruxelles (Belgium) following the protocol of Weis et al. (2006).

References

Ait-Hamou, F., Dautria, J.M., Cantagrel, J.M., Dostal, J., Briqueu, L., 2000. New geochronological and isotopic data on the Cenozoic volcanism of Ahaggar (southern Algeria): evidence for a mantle plume. Comptes Rendus de l'Académie des Sciences Série Ii Fascicule a-Sciences de la Terre et des Planètes 330, 829–836.

Allègre, C.J., Dupré, B., Lambret, B., Richard, P., 1981. The subcontinental versus suboceanic debate, I lead–neodymium–strontium isotopes in primary alkali basalts from a shield area the Ahaggar volcanic suite. Earth and Planetary Science Letters 52, 85–92.

Beccaluva, L., Azzouni-Sekkal, A., Benhallou, A., Bianchini, G., Ellam, R.M., Marzola, M., Siena, F., Stuart, F.M., 2007. Intracratonic asthenosphere upwelling and lithosphere rejuvenation beneath the Hoggar swell (Algeria): evidence from HIMU metasomatised lherzolite mantle xenoliths. Earth and Planetary Science Letters 260, 482–494.

Beccaluva, L., Bianchini, G., Ellam, R.M., Marzola, M., Oun, K.M., Siena, F., Stuart, F.M., 2008. The role of HIMU metasomatic components in the North African lithospheric mantle: petrological evidence from the Gharyan lherzolite xenoliths, NW Libya. Geological Society, London, Special Publications 293, 253–277.

Bensalah, M.K., Youbi, N., Mata, J., Madeira, J., Martins, L., El Hachimi, H., Bertrand, H., Marzoli, A., Bellieni, G., Doblas, M., Font, E., Medina, F., Mahmoudi, A., Beraâouz, E.H., Miranda, R., Verati, C., De Min, A., Ben Abbou, M., Zayane, R., 2013. The Jurassic–Cretaceous basaltic magmatism of the Oued El-Abid syncline (High Atlas, Morocco): physical volcanology, geochemistry and geodynamic implications. Journal of African Earth Sciences 81, 60–81.

Berger, J., Ennih, N., Liégeois, J.-P., Nkono, C., Mercier, J.-C.C., Demaiffe, D., 2008. A complex multi-chamber magmatic system beneath a late Cenozoic volcanic field: evidence from CSDs and thermobarometry of clinopyroxene from a single nephelinite flow (Djbel Saghro, Morocco). Geological Society of London, Special Publications 297, 509–524.

Berger, J., Ennih, N., Mercier, J.C.C., Liégeois, J.P., Demaiffe, D., 2009. The role of fractional crystallization and late-stage peralkaline melt segregation in the mineralogical evolution of Cenozoic nephelinites/phonolites from Saghro (SE Morocco). Mineralogical Magazine 73, 59–82.

Berger, J., Liégeois, J.-P., Ennih, N., Bonin, B., 2010. Flow of Canary mantle plume material through a subcontinental lithospheric corridor beneath Africa to the Mediterranean: comment. Geology 38, e202.

Berrahma, M., Delaloye, M., 1989. New geochronological data on the volcanic massif of Siroua (Anti-Atlas, Morocco). Journal of African Earth Sciences 1994 (9), 651–656.

Berrahma, M., Delaloye, M., Faure-Muret, A., Rachdi, H.E.N., 1993. Premieres donnees geochronologiques sur le volcanisme alcalin du Jbel Saghro, Anti-Atlas, Maroc. Journal of African Earth Sciences 17, 333–341.

Bezada, M.J., Humphreys, E.D., Davila, J.M., Carbonell, R., Harnafi, M., Palomeras, I., Levander, A., 2014. Piecewise delamination of Moroccan lithosphere from beneath the Atlas Mountains. Geochemistry, Geophysics, Geosystems 15, 975–985.

Bianchini, G., Beccaluva, L., Bonadiman, C., Nowell, G.M., Pearson, D.G., Siena, F., Wilson, M., 2010. Mantle metasomatism by melts of HIMU piclogite components: new insights from Fe-lherzolite xenoliths (Calatrava Volcanic District, central Spain). Geological Society, London, Special Publications 337, 107–124.

Bosch, D., Maury, R.C., El Azzouzi, M.h., Bollinger, C., Bellon, H., Verdoux, P., 2014. Lithospheric origin for Neogene–Quaternary Middle Atlas lavas (Morocco): clues from trace elements and Sr–Nd–Pb–Hf isotopes. Lithos 205, 247–265.

Bouabdellah, M., Hoernle, K., Kchit, A., Duggen, S., Hauff, F., Klügel, A., Lowry, D., Beaudoin, G., 2010. Petrogenesis of the eocene tamazert continental carbonatites (Central High Atlas, Morocco): implications for a common source for the tamazert and canary and Cape Verde island carbonatites. Journal of Petrology 51, 1655–1686.

Burkhard, M., Caritg, S., Helg, U., Robert-Charrue, C., Soulaimani, A., 2006. Tectonics of the Anti-Atlas of Morocco. Comptes Rendus - Academie des Sciences. Geoscience 338, 11.

Caby, R., 2003. Terrane assembly and geodynamic evolution of central-western Hoggar: a synthesis. Journal of African Earth Sciences 1994 (37), 133–159.

Chakhmouradian, A.R., Reguir, E.P., Kamenetsky, V.S., Sharygin, V.V., Golovin, A.V., 2013. Trace element partitioning in perovskite: implications for the geochemistry of kimberlites and other mantle-derived undersaturated rocks. Chemical Geology 353, 112–131.

Dasgupta, R., Hirschmann, M.M., Smith, N.D., 2007. Partial melting experiments of peridotite + CO_2 at 3 GPa and genesis of alkalic ocean island basalts. Journal of Petrology 48, 2093–2124.

Downes, H., Balaganskaya, E., Beard, A., Liferovich, R., Demaiffe, D., 2005. Petrogenetic processes in the ultramafic, alkaline and carbonatitic magmatism in the Kola Alkaline Province: a review. Lithos 85, 48–75.

Duggen, S., Hoernle, K.A., Hauff, F., Klugel, A., Bouabdellah, M., Thirlwall, M.F., 2009. Flow of Canary mantle plume material through a subcontinental lithospheric corridor beneath Africa to the Mediterranean. Geology 37, 283–286.

Ennih, N., Liégeois, J.-P., 2001. The Moroccan Anti-Atlas; the West African craton passive margin with limited Pan-African activity; implications for the northern limit of the craton. Precambrian Research 112, 289–302.

Ennih, N., Liégeois, J.P., 2008. The boundaries of the West African craton, with a special reference to the basement of the Moroccan metacratonic Anti-Atlas belt. Geological Society, London, Special Publications 297, 1–17.

Errami, E., Bonin, B., Laduron, D., Lasri, L., 2009. Petrology and geodynamic significance of the post-collisional Pan-African magmatism in the Eastern Saghro area (Anti-Atlas, Morocco). Journal of African Earth Sciences 1994 (55), 105–124.

Frey, F.A., Green, D.H., Roy, S.D., 1978. Integrated models of basalt petrogenesis: a study of quartz tholeiites to olivine melilitites from South Eastern Australia utilizing geochemical and experimental petrological data. Journal of Petrology 19, 463–513.

Frizon de Lamotte, D., Saint Bezar, B.A., Bracene, R., Mercier, E., 2000. The two main steps of the Atlas building and geodynamics of the western Mediterranean. Tectonics 19, 740–761.

Gasquet, D., Ennih, N., Liégeois, J.P., Soulaimani, A., Michard, A., 2008. The Pan-African Belt. In: Michard et al. (Ed.), Continental evolution: The Geology of Morocco 116. Lecture Notes in Earth Sciences, Springer Verlag, Berlin, pp. 33–64.

Green, D.H., 1970. A review of experimental evidence on the origin of basaltic and nephelinitic magmas. Physics of the Earth and Planetary Interiors 3, 221–235.

Green, T.H., Pearson, N.J., 1987. An experimental study of Nb and Ta partitioning between Ti-rich minerals and silicate liquids at high pressure and temperature. Geochimica et Cosmochimica Acta 51, 55–62.

Gurenko, A., Hoernle, K., Sobolev, A., Hauff, F., Schmincke, H.-U., 2010. Source components of the Gran Canaria (Canary Islands) shield stage magmas: evidence from olivine composition and Sr–Nd–Pb isotopes. Contributions to Mineralogy and Petrology 159, 689–702.

Harmand, C., Cantagrel, J.M., 1984. Le volcanisme alcalin Tertiaire et Quaternaire du Moyen Atlas (Maroc); chronologie K/Ar et cadre geodynamique. Journal of African Earth Sciences 2, 51–55.

Hauri, E.H., Wagner, T.P., Grove, T.L., 1994. Experimental and natural partitioning of Th, U, Pb and other trace elements between garnet, clinopyroxene and basaltic melts. Chemical Geology 117, 149–166.

Hay, D.E., Wendlandt, R.F., Wendlandt, E.D., 1995. The origin of Kenya rift plateau-type flood phonolites: evidence from geochemical studies for fusion of lower crust modified by alkali basaltic magmatism. Journal of Geophysical Research, Solid Earth 100, 411–422.

Herzberg, C., 2011. Identification of source lithology in the Hawaiian and Canary Islands: implications for origins. Journal of Petrology 52, 113–146.

Hirose, K., 1997. Partial melt compositions of carbonated peridotite at 3 GPa and role of CO_2 in alkali-basalt magma generation. Geophysical Research Letters 24, 2837–2840.

Hirose, K., Kushiro, I., 1993. Partial melting of dry peridotites at high pressures: determination of compositions of melts segregated from peridotite using aggregates of diamond. Earth and Planetary Science Letters 114, 477–489.

Hirschmann, M.M., Kogiso, T., Baker, M.B., Stolper, E.M., 2003. Alkalic magmas generated by partial melting of garnet pyroxenite. Geology 31, 481–484.

Hoepffner, C., Soulaimani, A., Pique, A., 2005. The Moroccan Hercynides. Journal of African Earth Sciences 1994 (43), 144–165.

Hoernle, K., Schmincke, H.U., 1993. The role of partial melting in the 15-Ma geochemical evolution of Gran-Canaria — a Blob Model for the Canary Hotspot. Journal of Petrology 34, 599–626.

Hofmann, A.W., 1997. Mantle geochemistry: the message from oceanic volcanism. Nature 385, 219–229.

Hofmann, A.W., Jochum, K.P., 1996. Source characteristics derived from very incompatible trace elements in Mauna Loa and Mauna Kea basalts, Hawaii scientific drilling project. Journal of Geophysical Research 101 (B5), 11.831–11.839.

Ibhi, A., Nachit, H., Abia, E.H., Hernandez, J., 2002. Intervention des segregats carbonatitiques dans la petrogenese des nephelinites a pyroxene de Jbel Saghro (Anti-Atlas, Maroc). Bulletin de la Societe Geologique de France 173, 37–43.

Kaszuba, J.P., Wendlandt, R.F., 2000. Effect of carbon dioxide on dehydration melting reactions and melt compositions in the lower crust and the origin of alkaline rocks. Journal of Petrology 41, 363–386.

Kogiso, T., Hirschmann, M.M., Frost, D.J., 2003. High-pressure partial melting of garnet pyroxenite: possible mafic lithologies in the source of ocean island basalts. Earth and Planetary Science Letters 216, 603–617.

LaTourrette, T., Hervig, R.L., Holloway, J.R., 1995. Trace element partitioning between amphibole, phlogopite, and basanite melt. Earth and Planetary Science Letters 135, 13–30.

Legendre, C., Maury, R.C., Caroff, M., Guillou, H., Cotten, J., Chauvel, C., Bollinger, C., Hemond, C., Guille, G., Blais, S., Rossi, P., Savanier, D., 2005. Origin of exceptionally abundant phonolites on Ua Pou Island (Marquesas, French Polynesia): partial melting of basanites followed by crustal contamination. Journal of Petrology 46, 1925–1962.

Liégeois, J.P., Latouche, L., Boughrara, M., Navez, J., Guiraud, M., 2003. The LATEA metacraton (Central Hoggar, Tuareg shield, Algeria): behaviour of an old passive margin during the Pan-African orogeny. Journal of African Earth Sciences 1994 (37), 161–190.

Liégeois, J.-P., Benhallou, A., Azzouni-Sekkal, A., Yahiaoui, R., Bonin, B., 2005. The Hoggar swell and volcanism; reactivation of the Precambrian Tuareg Shield during Alpine convergence and West African Cenozoic volcanism. Special Paper - Geological Society of America 388, 379–400.

Lucassen, F., Franz, G., Romer, R.L., Pudlo, D., Dulski, P., 2008. Nd, Pb, and Sr isotope composition of Late Mesozoic to Quaternary intra-plate magmatism in NE-Africa (Sudan, Egypt): high-mu signatures from the mantle lithosphere. Contributions to Mineralogy and Petrology 156, 765–784.

Lustrino, M., Wilson, M., 2007. The circum-Mediterranean anorogenic Cenozoic igneous province. Earth-Science Reviews 81, 1–65.

Lustrino, M., Cucciniello, C., Melluso, L., Tassinari, C.C.G., dè Gennaro, R., Serracino, M., 2012. Petrogenesis of Cenozoic volcanic rocks in the NW sector of the Gharyan volcanic field, Libya. Lithos 155, 218–235.

Mallik, A., Dasgupta, R., 2013. Reactive infiltration of MORB-eclogite-derived carbonated silicate melt into fertile peridotite at 3 GPa and genesis of alkalic magmas. Journal of Petrology 54, 2267–2300.

Malusà, M.G., Polino, R., Feroni, A.C., Ellero, A., Ottria, G., Baidder, L., Musumeci, G., 2007. Post-Variscan tectonics in eastern Anti-Atlas (Morocco). Terra Nova 19, 481–489.

Marks, M.A.W., Coulson, I.M., Schilling, J., Jacob, D.E., Schmitt, A.K., Markl, G., 2008. The effect of titanite and other HFSE-rich mineral (Ti-bearing andradite, zircon, eudialyte) fractionation on the geochemical evolution of silicate melts. Chemical Geology 257, 153–172.

Maza, M., Briqueu, L., Dautria, J.M., Bosch, D., 1998. The Achkal Oligocene ring complex: Sr, Nd Pb evidence for transition between tholeiitic and alkali Cenozoic magmatism in central Hoggar (south Algeria). Comptes Rendus de l'Académie des Sciences 327, 167–172.

McDade, P., Blundy, J.D., Wood, B.J., 2003. Trace element partitioning on the Tinaquillo Lherzolite solidus at 1.5 GPa. Physics of the Earth and Planetary Interiors 139, 129–147.

McDonough, W.F., Sun, S.S., 1995. The composition of the Earth. Chemical Geology 120, 223–253.

Missenard, Y., Cadoux, A., 2012. Can Moroccan Atlas lithospheric thinning and volcanism be induced by Edge-Driven Convection? Terra Nova 24, 27–33.

Missenard, Y., Zeyen, H., de Lamotte, D.F., Leturmy, P., Petit, C., Sebrier, M., Saddiqi, O., 2006. Crustal versus asthenospheric origin of relief of the Atlas Mountains of Morocco. Journal of Geophysical Research-Solid Earth 111.

Missenard, Y., Saddiqi, O., Barbarand, J., Leturmy, P., Ruiz, G., El Haimer, F.Z., de Lamotte, D.F., 2008. Cenozoic denudation in the Marrakech High Atlas, Morocco: insight from apatite fission-track thermochronology. Terra Nova 20, 221–228.
Natali, C., Beccaluva, L., Bianchini, G., Ellam, R.M., Siena, F., Stuart, F.M., 2013. Carbonated alkali-silicate metasomatism in the North Africa lithosphere: evidence from Middle Atlas spinel-lherzolites, Morocco. Journal of South American Earth Sciences 41, 113–121.
Olin, P.H., Wolff, J.A., 2012. Partitioning of rare earth and high field strength elements between titanite and phonolitic liquid. Lithos 128–131, 46–54.
Onuma, N., Ninomiya, S., Nagasawa, H., 1981. Mineral-groundmass partition-coefficients for nepheline, melilite, clinopyroxene and perovskite in melilite-nepheline basalt, Nyiragongo, Zaire. Geochemical Journal 15, 221–228.
Panter, K.S., J., B., Hart, S.R., Kyle, P.R., Esser, R., McIntosh, W.C., 2006. The origin of HIMU in the SW Pacific: evidence from intraplate volcanism in Southern New Zealand and Subantarctic islands. Journal of Petrology 47, 1673–1704.
Pfander, J.A., Munker, C., Stracke, A., Mezger, K., 2007. Nb/Ta and Zr/Hf in ocean island basalts — implications for crust-mantle differentiation and the fate of Niobium. Earth and Planetary Science Letters 254, 158–172.
Pilet, S., Baker, M.B., Stolper, E.M., 2008. Metasomatized lithosphere and the origin of alkaline lavas. Science 320, 916–919.
Pin, C., Briot, D., Bassin, C., Poitrasson, F., 1994. Concomitant separation of strontium and samarium-neodymium for isotopic analysis in silicate samples, based on specific extraction chromatography. Analytica Chimica Acta 298, 209–217.
Prowatke, S., Klemme, S., 2005. Effect of melt composition on the partitioning of trace elements between titanite and silicate melt. Geochimica et Cosmochimica Acta 69, 695–709.
Prowatke, S., Klemme, S., 2006. Trace element partitioning between apatite and silicate melts. Geochimica et Cosmochimica Acta 70, 4513–4527.
Rachdi, H., Berrahma, M., Delaloye, M., FaureMuret, A., Dahmani, M., 1997. Tertiary volcanism in Rekkame (Maroc): petrology, geochemistry and geochronology. Journal of African Earth Sciences 1994 (24), 259–269.
Raffone, N., Chazot, G., Pin, C., Vannucci, R., Zanetti, A., 2009. Metasomatism in the lithospheric mantle beneath Middle Atlas (Morocco) and the origin of Fe- and Mg-rich Wehrlites. Journal of Petrology 50, 197–249.
Rougier, S., Missenard, Y., Gautheron, C., Barbarand, J., Zeyen, H., Pinna, R., Liégeois, J.-P., Bonin, B., Ouabadi, A., Derder, M.E.-M., de Lamotte, D.F., 2013. Eocene exhumation of the Tuareg Shield (Sahara Desert, Africa). Geology 41, 615–618.
Salvi, S., Williams-Jones, A.E., 2006. Alteration, HFSE mineralisation and hydrocarbon formation in peralkaline igneous systems: insights from the Strange Lake Pluton, Canada. Lithos 91, 19–34.
Shaw, D.M., 1970. Trace element fractionation during anatexis. Geochimica et Cosmochimica Acta 34, 237–243.
Sobolev, A.V., Hofmann, A.W., Kuzmin, D.V., Yaxley, G.M., Arndt, N.T., Chung, S.-L., Danyushevsky, L.V., Elliott, T., Frey, F.A., Garcia, M.O., Gurenko, A.A., Kamenetsky, V.S., Kerr, A.C., Krivolutskaya, N.A., Matvienkov, V.V., Nikogosian, I.K., Rocholl, A., Sigurdsson, I.A., Sushchevskaya, N.M., Teklay, M., 2007. The amount of recycled crust in sources of mantle-derived melts. Science 316, 412–417.
Sorensen, H., 1997. The agpaitic rocks — an overview. Mineralogical Magazine 61, 485–498.
Stracke, A., Bizimis, M., Salters, V.J.M., 2003. Recycling oceanic crust: Quantitative constraints. Geochemistry Geophysics Geosystems 4, 33.
Tatsumi, Y., Arai, R., Ishizaka, K., 1999. The petrology of a melilite–olivine nephelinite from Hamada, SW Japan. Journal of Petrology 40, 497–509.
Teixell, A., Arboleya, M.L., Julivert, M., Charroud, M., 2003. Tectonic shortening and topography in the central High Atlas (Morocco). Tectonics 22, 1–13.
Teixell, A., Ayarza, P., Zeyen, H., Fernandez, M., Arboleya, M.-L., 2005. Effects of mantle upwelling in a compressional setting: the Atlas Mountains of Morocco. Terra Nova 17, 456–461.
Tesón, E., Teixell, A., 2008. Sequence of thrusting and syntectonic sedimentation in the eastern Sub-Atlas thrust belt (Dades and Mgoun valleys, Morocco). International Journal of Earth Sciences 97, 103–113.
Thomas, R.J., Chevallier, L.P., Gresse, P.G., Harmer, R.E., Eglington, B.M., Armstrong, R.A., de Beer, C.H., Martini, J.E.J., de Kock, G.S., Macey, P.H., Ingram, B.A., 2002. Precambrian evolution of the Sirwa Window, Anti-Atlas Orogen, Morocco. Precambrian Research 118, 1–57.
Thomas, R.J., Fekkak, A., Ennih, N., Errami, E., Loughlin, S.C., Gresse, P.G., Chevallier, L.P., Liegeois, J.P., 2004. A new lithostratigraphic framework for the Anti-Atlas Orogen, Morocco. Journal of African Earth Sciences 1994 (39), 217–226.
Urchulutegui, J.F., Fernandez, M., Zeyen, H., 2006. Lithospheric structure in the Atlantic-Mediterranean transition zone (southern Spain, northern Morocco): a simple approach from regional elevation and geoid data. Comptes Rendus - Academie des Sciences. Geoscience 338, 140–151.
Villemant, B., Jaffrezic, H., Joron, J.-L., Treuil, M., 1981. Distribution coefficients of major and trace elements; fractional crystallization in the alkali basalt series of Chaîne des Puys (Massif Central, France). Geochimica et Cosmochimica Acta 45, 1997–2016.
Wagner, C., Mokhtari, A., Deloule, E., Chabaux, F., 2003. Carbonatite and alkaline magmatism in Taourirt (Morocco): petrological, geochemical and Sr–Nd isotope characteristics. Journal of Petrology 44, 937–965.
Weis, D., Kieffer, B., Maerschalk, C., Barling, J., de Jong, J., Williams, G.A., Hanano, D., Pretorius, W., Mattielli, N., Scoates, J.S., Goolaerts, A., Friedman, R.M., Mahoney, J.B., 2006. High-precision isotopic characterization of USGS reference materials by TIMS and MC-ICP-MS. Geochemistry, Geophysics, Geosystems 7.
Weyer, S., Münker, C., Mezger, K., 2003. Nb/Ta, Zr/Hf and REE in the depleted mantle: implications for the differentiation history of the crust–mantle system. Earth and Planetary Science Letters 205, 309–324.
Wittig, N., Pearson, D.G., Duggen, S., Baker, J.A., Hoernle, K., 2010. Tracing the metasomatic and magmatic evolution of continental mantle roots with Sr, Nd, Hf and Pb isotopes: a case study of Middle Atlas (Morocco) peridotite xenoliths. Geochimica et Cosmochimica Acta 74, 1417–1435.
Wolff, J.A., 1984. Variation in Nb/Ta during differentiation of phonolitic magma, Tenerife, Canary Islands. Geochimica et Cosmochimica Acta 48, 1345–1348.